

1 **Title**

2 Scalable Multi-Sample Single-Cell Data Analysis by Partition-Assisted Clustering and Multiple
3 Alignments of Networks

4

5 **Authors**

6 Ye Henry Li^{a,*}, Dangna Li^{b,*}, Nikolay Samusik^c, Xiaowei Wang^d, Leying Guan^d, Garry P. Nolan^c, Wing
7 Hung Wong^{d,e,1}

8 *Equal Contribution: Y.H.L and D.L.

9 ¹To whom correspondence should be addressed. Email: whwong@stanford.edu

10

11 **Author Affiliations**

12

13 Ye Henry Li

14 ^aStructural Biology Department and Public Policy Program, Stanford University, Stanford, USA.

15

16 Dangna Li

17 ^bInstitute for Computational and Mathematical Engineering, Stanford University, Stanford, USA.

18

19 Nikolay Samusik

20 ^cDepartment of Microbiology and Immunology, Baxter Laboratory, Stanford University, Stanford, USA

21

22 Garry P. Nolan

23 ^cDepartment of Microbiology and Immunology, Baxter Laboratory, Stanford University, Stanford, USA

24

25 Xiaowei Wang

26 ^dStatistics Department, Stanford University, Stanford, USA.

27

28 Leying Guan

29 ^dStatistics Department, Stanford University, Stanford, USA.

30

31 Wing Hung Wong

32 ^dStatistics Department, Stanford University, Stanford, USA.

33 ^eDepartment of Biomedical Data Science, Stanford University, Stanford, USA

34

35 **Contributions**

36 Y.H.L. and W.H.W. conceived the project. Y.H.L., D.L., L.G. and W.H.W. designed the data analysis
37 pipeline; Y.H.L. and D.L. implemented the data analysis pipeline. N.S. generated the hand-gated CyTOF
38 data. Y.H.L., D.L., N.S., and X.W. analyzed the data. Y.H.L., D.L., N.S. and W.H.W. wrote the
39 manuscript and developed the figures. G.P.N and W.H.W. supervised the study.

40

41 **Conflict of Interest**

42 The authors declare no conflict of interest.

43

44

45

46

47

48

49

50

51

52

53

54

55 Abstract

56 Mass cytometry (CyTOF) has greatly expanded the capability of cytometry. It is now easy to generate
57 multiple CyTOF samples in a single study, with each sample containing single-cell measurement on 50
58 markers for more than hundreds of thousands of cells. Current methods do not adequately address the
59 issues concerning combining multiple samples for subpopulation discovery, and these issues can be
60 quickly and dramatically amplified with increasing number of samples. To overcome this limitation, we
61 developed Partition-Assisted Clustering and Multiple Alignments of Networks (PAC-MAN) for the fast
62 automatic identification of cell populations in CyTOF data closely matching that of expert manual-
63 discovery, and for alignments between subpopulations across samples to define dataset-level cellular
64 states. PAC-MAN is computationally efficient, allowing the management of very large CyTOF datasets,
65 which are increasingly common in clinical studies and cancer studies that monitor various tissue samples
66 for each subject.

67

68 Introduction

69 Analyses of CyTOF data rely on many of the tools and ideas from flow cytometry (FC) data analysis, as
70 CyTOF datasets are essentially higher dimensional versions of flow cytometry datasets. Currently, the
71 most widely used method in FC is still human hand-gating, as other methods often fail to extract
72 meaningful subpopulations of cells automatically. In hand-gating, we draw polygons or other enclosures
73 around pockets of cell events on a two-dimensional scatterplot to define subpopulations and cellular states
74 that are observed in the data. This process is painfully time-consuming and requires advance knowledge
75 of the marker panel design, the quality of the staining reagents, and, most importantly, *a priori* what cell
76 subpopulations to expect to occur in the data. When presented with a new set of marker panels and
77 biological system, the researcher would find it difficult to delineate the cell events, especially in high-
78 dimensional and multiple-sample datasets.

79 The inefficient nature of hand-gating in flow cytometry motivated algorithmic development in automatic
80 gating. Perhaps the most popular is flowMeans(1), which is optimized for FC and can learn
81 subpopulations in FC data(2) in an automated manner; however, it has not been successfully applied to
82 CyTOF data analysis. Currently, most data analysis tools created for flow cytometry data analyses are not
83 easily applicable for high-dimensional datasets(3). An exception is SPADE, which was developed and
84 optimized specifically for the analysis of CyTOF datasets(3). flowMeans and SPADE constitute the
85 leading computational methods in cytometry, but as shown later in this work, their performance may
86 become sub-optimal when challenged with large and high-dimensional datasets. There are also other
87 recent clustering-based tools that utilize dimensionality reduction and projections of high-dimensional
88 data, however, these tools do not directly learn the subpopulations for all the cell events, and may be too
89 slow to complete data analysis for an increasing amount of samples.

90 In this study, we address the data analysis challenges in two major steps. First, we propose the partition-
91 assisted clustering (PAC) approach, which produces a partition of the k -dimensional space (k =number of
92 markers) that captures the essential characteristic of the data distribution. This partitioning methodology
93 is grounded in a strong mathematical framework of partition-based high-dimensional density
94 estimation(4–8). The mathematical framework offers the guarantee that these partitions approximate the

95 underlying empirical data distribution; this step is faster than the recent k-nearest neighbor-based method
96 (9) and is essential to the scalability of our clustering approach to analyze datasets with many samples.
97 The clustering of cells based on recursive partitioning is then refined by a small number of k-means style
98 iterations before a merging step to produce the final clustering.

99 Secondly, the subpopulations learned separately in multiple different but related datasets can be aligned
100 by marker network structures (multiple alignments of networks, or MAN), making it possible to
101 characterize the relationships of subpopulations across different samples automatically. The ability to do
102 so is critical for monitoring changes in a subpopulation across different conditions. Importantly, in every
103 study, batch effect is present; batch effects shift subpopulation signals so that the means can be different
104 from experiment to experiment. PAC-MAN naturally addresses batch effects in finding the alignments of
105 the same or closely related subpopulations from different samples.

106 PAC-MAN finds homogeneous clusters efficiently with all data points in a scalable fashion and enables
107 the matching of these clusters across different samples to discover cluster relationships in the form of
108 clades.

109

110 **Results and Discussion**

111

112 *PAC*

113 PAC has two parts: partitioning and post-processing. In the partitioning part of PAC, the data space is
114 recursively divided into smaller hyper-rectangles based on the number of data points in the locality
115 (Figure 1a). The partitioning is accomplished by either Bayesian Sequential Partition (BSP) with limited
116 look-ahead (Figure 1a and 1b) or Discrepancy Sequential Partition (DSP) (Figure 1a); these are two fast
117 variants of partition-based density estimation methods previously developed by our group (4–8), with
118 DSP being the fastest. BSP and DSP divide the sample space into hyper-rectangles with uniform density
119 value in each of them. The subsetting of cells according to the partitioning provides a principled way of
120 clustering the cells that reflects the characteristics of the underlying distribution. In particular, each
121 significant mode is captured by a number of closely located rectangles with high-density values (Figure
122 1c). Although this method allows a fast and unbiased localization of the high-density regions of the data
123 space, we should not use the hyper-rectangles directly to define the final cluster boundaries for two
124 reasons. First, real clusters are likely to be shaped elliptically, therefore, the data points in the corners of a
125 hyper-rectangle are likely to be incorrectly clustered. Second, a real cluster is often split into more than
126 one closely located high-density rectangles. We designed post-processing steps to overcome these
127 limitations: 1) a small number of k-means iterations is used to round out the corners of the hyper-
128 rectangles, 2) a merging process is implemented to ameliorate the splitting problem, which is inspired by
129 the flowMeans algorithm. The details of post-processing are given in Materials and Methods. The
130 resulting method is named b-PAC or d-PAC depending on whether the partition is produced by BSP or
131 DSP.

132

133 *MAN*

134 An approach to analyze multiple related samples of CyTOF data is to pool all samples into a combined
135 sample before detection of subpopulations. This is a natural approach under the assumptions that there are
136 no significant batch effects or systematic shifts in cell subpopulations across the different samples.
137 However, such assumptions may not hold due to one or more of the following reasons:

- 138 1) Dataset size and instruments used. Large number of samples usually means the samples were
139 collected on different days with different experimental preparations. Many steps can introduce
140 significant shifts in measurement levels.
- 141 2) Staining reagents. Reagents such as antibodies, purchased from different vendors and batch
142 preparations can affect the overall signal. While saturation of reagents in the protocol could help
143 eliminate the batch effects in the staining procedure, this approach is costly and might not work
144 for all antibodies, especially those with poor specificity.
- 145 3) Normalization beads stock. While normalization beads(10) help to control for the signal level,
146 especially within one experiment, the age of the beads stock and their preparation could lead to
147 significant batch effects. In addition, there are different types of normalization beads and
148 normalization calculations.
- 149 4) Human work variation. While many researchers are studying the same system (e.g., immune
150 system), different protocols and implementation by different researchers, who sometimes perform
151 experimental steps slightly differently, can lead to batch effects.
- 152 5) Subpopulation dynamics. The subpopulation centers can move from sample to sample due to
153 treatments on the cells in treatment-control studies or perturbation studies. General practice is to
154 cluster by phenotypic markers.
- 155 6) Sample background. If the data came from different cell lines or individuals in a clinical study,
156 the measurement levels and proportions of cell subpopulations would be expected to change from
157 sample to sample. Without expert scrutiny, it would be difficult to make sense of the data with
158 current data analysis tools.

159 Could we extract shared information that allows us to interpret cross-sample similarities and differences?
160 To ameliorate these difficulties, we have designed an alternative approach that is effective in the presence
161 of substantial systematic between-sample variation. In this approach, each sample is analyzed separately
162 (by PAC) to discover within-sample subpopulations. Over-partitioning in this step is allowed in order not
163 to miss small subpopulations. The subpopulations from all samples are then compared to each other based
164 on a pairwise dissimilarity measure designed to capture the differences in within-sample distributions
165 (among the markers) across two subpopulations. Using this dissimilarity, we perform bottom-up
166 hierarchical clustering of the subpopulations to represent the relationship among the subpopulations. The
167 resulting tree of subpopulations is then used to guide the merging of subpopulations from the same
168 sample, and to establish linkage of related subpopulations from different samples. We note that the design
169 of a dissimilarity measure (Materials and Method) that is not sensitive to systematic sample-to-sample
170 variation is a novel aspect of our approach. The merging of subpopulations from the same sample is also
171 important, as it offers a way to correct any over-partitioning that may have occurred during the initial
172 PAC analysis of each sample. We emphasize that, as with the usage of all statistical methods, the user
173 must utilize samples or datasets that are considered as good as possible; interpretation of the analysis
174 results rely on the researchers to collect data with validated reagents for all samples.

175

176 *Rational initialization for PAC increases clustering effectiveness*

177 Appropriate initialization of clustering is very important for eventually finding the optimal clustering
178 labels; PAC works well because the implicit density estimation procedure yields rational centers to learn
179 the modes of sample subpopulations. When tested on the hand-gated CyTOF data on the bone marrow
180 sample in (14), compared to k-means alone, PAC gives lower total sums of squares and higher F-
181 measures in the subpopulations (Figure 1d and 1e). This process also helps PAC to converge in 50
182 iterations (Figure 1f) in post-processing, whereas k-means performs very poorly even after 5000 iterations
183 (Figure 1g). Through the lens of t-sne plots (Figure 1g), the PAC results are more similar to the hand-
184 gating results, while the k-means, flowMeans, and SPADE clustering results perform poorly. In
185 flowMeans, several large subpopulations are merged. SPADE's separation of points is inconsistent and
186 highly heterogeneous, probably due to its down-sampling nature. On the other hand, by inspection, PAC
187 obtains similar separation for both the major and minor subpopulations as the hand-gating results.

188

189 *PAC is consistently better than flowMeans and SPADE for simulated datasets and hand-gated cytometry*
190 *datasets*

191 In the systematic simulation study, we challenged the methods with different datasets with varying
192 number of dimensions, number of subpopulations, and separation between the subpopulations. The F-
193 measure and p-measures for the PAC methods are consistently equal or higher than that of flowMeans
194 and SPADE (Table 1 and Supporting Figure 2a). In addition, we observe that flowMeans gives
195 inconsistent F-measures for similar datasets (Table 1), which may be due to the convergence of k-means
196 to a local minimum without a rational initialization.

197 Next, we tested the methods based on published hand-gated cytometry datasets to see how similar the
198 estimated subpopulations are to those obtained by human experts. We applied the methods on the
199 hematopoietic stem cell transplant and Normal Donors datasets from the FlowCAP challenges(2) and on
200 the subset of gated mouse bone marrow CyTOF dataset (Dataset 5) recently published(11). The gating
201 strategy of the CyTOF dataset is provided in Supporting Figure 1. The dataset and expert gating strategy
202 are the same as described earlier(12). Note that in the flow cytometry data, the computed F-measures are
203 slightly lower than that reported in FlowCAP; this is due to the difference in the definition of F-measures.
204 Overall, the PAC outperforms flowMeans and SPADE by consistently obtaining higher F-measures
205 (Table 1). In particular, in the CyTOF data example, PAC generated significantly higher F-measures
206 (greater than 0.82) than flowMeans and SPADE (0.59 and 0.53, respectively). In addition, PAC gives
207 higher overall subpopulation-specific purities (Supporting Figure 2b and Supporting Table 1). These
208 results indicate that PAC gives consistently good results for both low and high-dimensional datasets.
209 Furthermore, PAC results match human hand-gating results very well. The consistency between PAC-
210 MAN results and hand-gating results in this large data set confirms the practical utility of the
211 methodology.

212

213 *Separate-then-combine outperforms Pool Approach when Batch Effect is present*

214 It is natural to analyze samples separately then combine the subpopulation features for downstream
215 analysis in the multiple samples setting. However, we need to resolve the batch effects.
216 Two distinct subpopulations could overlap in the combined/pooled sample, such as in the case when the
217 data came from two generations of CyTOF instruments (newer instrument elevates the signals). On the
218 other hand, in cases with changing means, two subpopulations can evolve together such that their means
219 change slightly, but enough to shadow each other when samples are merged prior to clustering.

220 First, we consider the overlapping scenario (Figure 2b). When viewed together in the merged sample, the
221 right subpopulation from sample 1 overlaps with the left subpopulation in sample 2 (Figure 2c). There is
222 no way to use expression level alone to delineate the two overlapping subpopulations (Figure 2d). By
223 learning more subpopulations using PAC, there are some hints that multiple subpopulations are present
224 (Figure 2e). Despite these hints, it would not be possible to say whether the shadowed subpopulations
225 relate in any way to other distinct subpopulations.

226 PAC-MAN resolves the overlapping issue by analyzing the samples separately (Figure 2f). Considering
227 the case in which we do not know *a priori* the number of true subpopulations, we learn three
228 subpopulations per sample. The network structures of the subpopulations discovered are presented in
229 Figure 2g and we see that the third subpopulations from the two samples share the same network
230 structures, while the first subpopulations of the two samples differ by only one edge; these respective
231 networks are clustered together in the dendrogram (Figure 2h, bottom panel). By utilizing the networks,
232 the clades that represent the same and/or similar subpopulations of cells can be established. Clustering by
233 network structures alone resolves the majority of points in the data (Figure 2h, top panel). Furthermore, as
234 discussed next, by incorporating marker levels into the alignment process, all the points can be resolved
235 (Figure 2i).

236 Next we consider the case with dynamic evolution of subpopulations that models the treatment-control
237 and perturbation studies. The interesting information is in tracking how subpopulations change over the
238 course of the experiment. In the simulation, we have generated two subpopulations that nearly converge
239 in mean expression profile over the time course (Figure 3a). The researcher could lose the dynamic
240 information if they were to combine the samples for clustering analysis. As in the previous case, we could
241 use PAC to learn several subpopulations per sample (Figure 3b). Then, with the assumption that there are
242 two evolving clusters from data exploration, we align the subpopulations to construct clades of same
243 and/or similar subpopulations (Figure 3c) based on the network structural information (Supporting Figure
244 3). With network and expression level information in the alignment process, the two subpopulations or
245 clades can be resolved naturally (Figure 3c).

246

247 *Network and expression alignment is better than network or expression alignment alone*

248 With networks in hand, we could further characterize the relationships between subpopulations across
249 samples. However, the alignment process needs to work well for true linkage to be established. We could
250 align by network alone, by expression (or marker) means, or both. Figures 2h, 2i, and 3c present these
251 alternatives in comparison. By using all the subpopulation networks, the results still contain subsets of
252 misplaced cells (Figures 2h top panel and 3c left panel). This is because small clusters of cells have noisy
253 underlying covariance structure; therefore, the networks cannot be accurately inferred. These structural

254 inaccuracies negatively impact the network clustering. The (mean) marker level approach also does not
255 work well (Figure 3c center panel) due to the subpopulation mean shifts across samples. On the other
256 hand, the sequential approach works well (Figures 2i and 3c right panel). In the sequential approach,
257 larger (>1500 in batch effect case; >1000 in dynamic case) subpopulations' networks are utilized for the
258 initial alignment process. Next, the smaller subpopulations, which have noisy covariance, are merged
259 with the closest larger, aligned subpopulations. Thus, more subpopulations could be discovered upstream
260 (in PAC), and the network alignment would work similarly as the smaller subpopulations, which could be
261 fragments of a distribution, do not impact the alignment process (Supporting Figure 4a and b). Moreover,
262 in the network inference step, unimportant edges can negatively impact the alignment process (Supporting
263 Figure 4c) in the network-alone case. Biologically, this means that edges that do not constrain or define
264 the cellular state should not be utilized in the alignment of cellular states. Effectively, the threshold placed
265 on the number of edges in the network inference controls for the importance of the edges. Thus, the
266 combined alignment approach works well and allows moderate over-saturation of cellular states to be
267 discovered in the PAC step so that no advance knowledge of the exact number of subpopulations is
268 necessary.

269

270 *PAC-MAN efficiently outputs meaningful data-level subpopulations for mouse tissue dataset*

271

272 We use the recently published mouse tissue dataset(11) to illustrate the multi-sample data analysis
273 pipeline. The processed dataset contains a total of more than 13 million cell events in 10 different tissue
274 samples, and 39 markers per event (Supporting Table 2). The original research results centered on
275 subpopulations discovered from hand-gating the bone marrow tissue data to find 'landmark'
276 subpopulations; the rest of the data points were clustered to the most similar landmark subpopulations.
277 While this enables the exploration of the overall landscape from the perspective of bone marrow cell
278 types, a significant amount of useful information from the data remains hidden.

279 In contrast, using d-PAC-MAN, the fastest approach by our comparison results, we can perform
280 subpopulation discovery for each sample automatically and then align the subpopulations across samples
281 to establish dataset-level cellular states. On a standard Core i7-44880 3.40GHz PC computer, the single-
282 thread data analysis process with all data points takes about one hour to complete, which is much faster
283 than alternative methods. With multi-threading and parallel processing, the data analysis procedure can be
284 completed very quickly. As mentioned earlier, PAC results for the bone marrow subsetted data from this
285 dataset matches closely to that of the hand-gated results. This accuracy provides confidence for applying
286 PAC to the rest of the dataset.

287 Figure 4 shows the t-sne plots for subpopulation discovered (top panel of each sample) and the
288 representative subpopulation established (bottom panel of each sample) for the entire dataset. In the PAC
289 discovery step, we learn 35 subpopulations per sample without advance knowledge of how many
290 subpopulations are present. This moderate over-partitioning of the data samples leads to a moderate
291 heterogeneity in the t-sne plots. Next, the networks are inferred for the larger subpopulations (with
292 number of cell events greater than 1000), and the networks are aligned for all the tissue samples. We
293 output 80 representative subpopulations or clades for the entire dataset to account for the traditional

294 immunological cellular states and sample-specific cellular states present. Within samples, the
295 subpopulations that cluster together by network structure are aggregated. The smaller subpopulations (not
296 involved in network alignment) are either merged to the closest larger subpopulation or establish their
297 own sample-specific subpopulation by expression alignment; small subpopulations were clamped with
298 larger clades by grouping the subpopulations into 5 clusters per sample based on the means (of marker
299 signal). The representative subpopulations (90 total) follow the approximate distribution of the cell events
300 on the t-sne plots and the aggregating effect cleans up the heterogeneities due to over-partitioning in the
301 PAC step.

302 The cell type clades are the representative subpopulations for the entire dataset, and they could either be
303 present across samples or in one sample alone. Their distribution is visualized by a heatmap (Figure 5).
304 While the bone marrow sample contains many cell types, only a subset of them are directly aligned to cell
305 types in other samples, which means using the bone marrow data as the reference point leaves much
306 information unlocked in the dataset. The cell types in the blood and spleen samples have more alignments
307 with cell types in other samples. The lymph node samples share many clades; the small intestine and
308 colon samples also share many clades, probably due to closeness in biological function. The thymus
309 sample has few clades shared with other samples, which may be due to its functional specificity.

310 PAC-MAN style analysis can be applied to align the tissue subpopulations by their means instead of
311 network similarities (Supporting Figure 5). As done previously, representative clades (88 total) were
312 outputted. The same aggregating effect is observed (Supporting Figure 5a), and this is due to the
313 organization from dataset-level variation in the means. Comparing to the network alignment, the means
314 linkage approach has slightly more subpopulations per sample; the subpopulation proportion heatmap
315 (Supporting Figure 5b) shows more linking. Although the bone marrow sample subpopulations co-occur
316 in the same clades slightly more with other sample subpopulations, this sample does not co-occur with
317 many clades in the dataset. Thus, a PAC-MAN style analysis with means linkage also harvests additional
318 information from the entire dataset.

319 To compare the network and means approaches with PAC-MAN, we study the F-measure and p-measure
320 results with 88 total clades from each approach. The overall F-measure with all cell events is 0.7969 and
321 the overall F-measure with clades assignments of PAC-discovered subpopulations is 0.3143. The two F-
322 measure values suggest that the assignment of PAC-discovered subpopulations is more consistent for
323 larger subpopulations.

324 To illustrate the assignment purities, the p-measures are computed for the following two cases. 1)
325 Network clade assignment is the basis (network-justified), similar to the ground truth in the clustering
326 comparisons previously; or 2) means clade assignment is the basis (means-justified) (Supporting Table 4).
327 P-measure cutoff is set at 0.3 (to remove unreliable comparisons) to obtain purer clade assignments. In the
328 network-justified case, PAC subpopulations with more than 0.3 in p-measure constitute 93.44 % of all
329 cell events. In the means-justified case, PAC subpopulations with more than 0.3 in p-measure constitute
330 92.67 % of all cell events. Furthermore, if the p-measure cutoff were to increase to 0.5, the percentages of
331 cells left for the network-justified and mean-justified cases are 6.25% and 75.16%, respectively. The
332 network-justified case yields drastically lower numbers of cell events in the purer PAC subpopulations
333 because the means approach has more heterogeneity in the linkages (defined as PAC-subpopulation
334 participants in each shared clade with size of at least 2). In fact, the network approach has 100 linkages

335 while the means approach has 209 linkages. Therefore, the extra linkages in the means approach would
336 yield greater impurities in the network-justified case. The linkage plot (Supporting Figure 6a) shows that
337 the low linkages occur slightly more frequently for the network approach. One consequence is that the
338 network approach aggregates PAC subpopulations within sample more frequently; for instance, in the
339 thymus sample, the network approach yields 14 clades while the means approach yields 21 clades.

340 After aggregating, the clade sizes (with unique participants per sample) are plotted (Supporting Figure
341 6b). The network approach tends to find fewer linkages, as more clades have sizes of less than 4, while
342 the means approach has more clades than the network approach with clade sizes greater than 4. The
343 network approach is more conservative due to the additional constraints from network structures.
344 Conventionally, in the cytometry field, only the means are considered in the definition of cellular states.
345 Assuming the absence of batch and dynamic effects, the researcher could view the purer shared clade
346 assignments in the network-justified case (general agreement between constrained network approach and
347 means approach) as more reliable candidates of cross-sample relationships to investigate in future
348 experiments (Supporting Figure 6c).

349 Hence, the network alignment approach is in agreement that of the means approach, with network
350 alignment being more stringent in the establishment of linkages. The network PAC-MAN approach
351 defines cellular states with the additional information from network structures, and it has the effect of
352 constraining the number of linkages between samples while finding linkages for subpopulations that are
353 distant in their means.

354

355 *Network hubs provide natural annotations*

356 To further characterize the cell types, we annotate the clades within each sample using the top network
357 hub markers, which constrain the cellular states. The full annotation, along with mean average expression
358 profiles, is presented in Supporting Table 3. The clade information is presented in the ClusterID column.
359 The annotations for cells across different samples but within the same clades share hub markers. For
360 example, in clade 1 for the blood and bone marrow samples, the cells share the hub markers Ly6C and
361 CD11b. In the bone marrow sample, one important set of subpopulations is the hematopoietic stem cell
362 subpopulations. One such subpopulation is present as clade 18 with the annotation CD34-CD27-cKit-
363 Sca1 and is about 1.87 percent in the bone marrow sample. Clade 18 is only present in the bone marrow
364 sample, indicating that the PAC-MAN pipeline defines this as a sample-specific and coherent
365 subpopulation using dataset-level variation. The thymus contains a large subpopulation (84.07 percent)
366 that is characterized as CD5-CD4-CD43-CD3, suggesting it to be the maturing T-cell subpopulation.

367

368 **Conclusion**

369 We have presented the PAC-MAN data analysis pipeline. This pipeline was designed to remove major
370 roadblocks in the utilization of existing and future CyTOF datasets. First, we established a quick and
371 accurate clustering method that closely matches expert gating results; second, we demonstrated the
372 management of multiple samples by handling mean shifts and batch effects across samples. The
373 alignment allows researchers to find relationships between cells across samples without resorting to

374 pooling of all data points. This pipeline can be efficiently utilized to analyze large datasets of high-
375 dimension. PAC-MAN allows the cytometry field to harvest information from the increasing amount of
376 CyTOF data available.

377

378 **Materials and Methods**

379

380 *Partition-assisted clustering has two parts*

381 1) Partitioning: a partition method (BSP(5) or DSP(7)) is used to learn N initial cluster centers from the
382 original data.

383 2) Post-processing: A small number (m) of k-mean iterations is applied to the rectangle-based clusters
384 from the partitioning, where m is a user-specified number. We used m=50 in our examples. After this k-
385 means refinement, we merge the N clusters hierarchically until the desired number of clusters (this
386 number is user-specified) is reached. The merging is based on a given distance metric for clusters. In the
387 current implementation, we use the same distant metric as in flowMeans(1). That is, for two clusters X
388 and Y, their distance $D(X, Y)$ is defined as:

$$D(X, Y) = \min \{(\bar{x} - \bar{y})^T S_x^{-1} (\bar{x} - \bar{y}), (\bar{x} - \bar{y})^T S_y^{-1} (\bar{x} - \bar{y})\}$$

389 where \bar{x}, \bar{y} are the sample mean of cluster X and Y, respectively. S_x^{-1} is the inverse of the sample
390 covariance matrix of cluster X. S_y^{-1} is defined similarly. In each step of the merging process, the two
391 clusters having the smallest pairwise distance will be merged together into one cluster.

392

393 *Partition Methods*

394 There are two partition methods implemented in the comparison study: d-PAC and b-PAC. The results
395 are similar, with d-PAC being the faster algorithm. Figure 1a illustrates this recursive process.

396 d-PAC is based on the discrepancy density estimation (DSP)(7). Discrepancy, which is widely used in the
397 analysis of Quasi-Monte Carlo methods, is a metric for the uniformity of points within a rectangle. DSP
398 partitions the density space recursively until the uniformity of points within each rectangle is higher than
399 some pre-specified threshold. The dimension and the cut point of each partition are chosen to
400 approximately maximize the gap in uniformity of two adjacent rectangles.

401 BSP + LL is an approximation inference algorithm for Bayesian sequential partitioning density estimation
402 (BSP)(5). It borrows ideas from Limited-Look-ahead Optional Pólya Tree (LL-OPT), an approximate
403 inference algorithm for Optional Pólya Tree(8). The original inference algorithm for BSP looks at one
404 level ahead (i.e. looking at the possible cut points one level deeper) when computing the sampling
405 probability for the next partition. It then uses resampling to prune away bad samples. Instead of looking at
406 one level ahead, BSP + LL looks at h levels ahead ($h > 1$) when computing the sampling probabilities for
407 the next partition and does not do resampling (Figure 1b). In other words, it compensates the loss from

408 not performing resampling with more accurate sampling probabilities. For simplicity, ‘BSP + LL’ is
409 shortened to ‘BSP’ in the rest of the article.

410

411 *F-measure*

412 We use the F-measure for comparison of clustering results to ground truth (known in simulated data, or
413 provided by hand-gating in real data). This measure is computed by regarding a clustering result as a
414 series of decisions, one for each pair of data points. A true positive decision assigns two points that are in
415 the same class (i.e. same class according to ground truth) to the same cluster, while a true negative
416 decision assigns two points in different classes to different clusters. The F-measure is defined as the
417 harmonic mean of the precision and recall. Precision P and recall R are defined as:

418 $P = \frac{TP}{TP+FP}$, $R = \frac{TP}{TP+FN}$, where TP is the total number of true positives, FP is the total number of false
419 positives and FN is the total number of false negatives.

420 F-measure ranges from 0 to 1. The higher the measure, the more similar the estimated cluster result is to
421 the ground truth. This definition of F-measure is different than that of FlowCAP challenge(2). The use of
422 co-assignment of labels in this definition is a more accurate way to compute the true positives and
423 negatives.

424

425 *Purity-measure (p-measure)*

426 Most of the existing measurements for clustering accuracy aim at measuring the overall accuracy of the
427 entire datasets, i.e. comparing with the ground truth over all clusters. However, we are also interested in
428 analyzing how well a clustering result matches the ground truth within a certain class. Specifically,
429 consider a dataset D with K classes: $\{C_1, C_2, \dots, C_K\}$ and a given ground truth cluster labels g, we construct
430 an index called the purity measure, or p-measure for short, to measure how well our clustering result
431 matches g for each class C_i . This index is computed as follows:

432 1) For each class C_k , look for the cluster that has the maximum number of overlapping points with this
433 class, denoted by L_{i_k} .

434 2) Define $S_1 = \frac{|C_k \cap L_{i_k}|}{|L_{i_k}|}$, $S_2 = \frac{|C_k \cap L_{i_k}|}{|C_k|}$, where $|\cdot|$ denotes the number of points in a set.

435 3) The final P-index for class C_k is given by: $P = \frac{2S_1S_2}{S_1+S_2}$.

436 If we were to match a big cluster with a small class, even though the overlapping may be large, S_1 would
437 still be low since we have divided the score by the size of the cluster in S_1 . In addition, we are interested
438 in knowing how many points in C_k are clustered together by L_{i_k} , which is measured by S_2 .

439

440 *Network construction and comparison*

441 After PAC, the discovered subpopulations typically have enough cells for the estimation of mutual
442 information. This enables the construction of networks as the basis for cell type characterization.
443 Computationally, it is not good to directly use the mutual information networks constructed this way to
444 organize the subpopulations downstream. The distance measure used to characterize the networks could
445 potentially give the same score for different network structures. Thus, it is necessary to threshold the
446 network edges based on the strength of mutual information to filter out the noisy and miscellaneous
447 edges. In this work, these subpopulation-specific networks are constructed using the MRNET network
448 inference algorithm in the Parmigene (13) R package. The algorithm is based on mutual information
449 ranking, and outputs significant edges connecting the markers. The top d edges (d is set to be 1x the
450 number of markers in all examples) are used to define a network for the subpopulation. This process
451 enables a careful calculation of the distance measure.

452 For each pair of subpopulation networks, we calculate a network distance, which is defined as follows. If
453 G_1 and G_2 are two networks, let S be the set of shared edges and A be union of the of the edges in the two
454 networks, then we define

455
$$\text{Similarity}(G_1, G_2) = \frac{|S|}{|A|}, \text{ where } |\cdot| \text{ denotes the size of a set.}$$

456 This is known as the Jaccard coefficient of the two graphs. The Jaccard distance, or 1- Jaccard coefficient,
457 is then obtained. This is a representation of the dissimilarity between each pair of networks; the Jaccard
458 dissimilarity is the measure used for the downstream hierarchical clustering.

459

460 *Cross-sample linkage of subpopulations*

461 We perform agglomerative clustering of the pool of subpopulations from all samples. This clustering
462 procedure greedily links networks that are the closest in Jaccard dissimilarity, and yields a dendrogram
463 describing the distance relationship between all the subpopulations. We cut the dendrogram to obtain the
464 k clades of subpopulations. Subpopulations from the same sample and falling into the same clade are then
465 merged into a single subpopulation (Figure 2a). This merging step has the effect of consolidating the
466 over-partitioning in the PAC step. No merging is performed for subpopulations from different samples
467 sharing the same clade. In this way, we obtain k clades of subpopulations, with each clade containing no
468 more than one subpopulation from each sample. We regard the subpopulations within each clade as being
469 linked across samples.

470 In the above computation, only subpopulations with enough cells to define a stable covariance are used
471 for network alignment via the Jaccard distance; the rest of the cell events from very small subpopulations
472 are then merged with the closet clade by marker profile via distance of mean marker signals. If the small
473 subpopulations are distant from the defined clades, then a new sample-specific clade is created for these
474 small subpopulations.

475

476

477 *Annotation of Subpopulations*

478 To annotate the cellular states, we first apply PAC-MAN to learn the dataset-level subpopulation/clade
479 labels. Next, these labels are used to learn the representative/clade networks. The top hubs (i.e. the most
480 connected nodes) in these networks are used for annotation. This approach has biological significance in
481 that important markers in a cellular state are often central to the underlying marker network, which is
482 analogous to important genes in gene regulatory networks; these important markers have many
483 connections with other markers. If the connections were broken, the cell would be perturbed and
484 potentially driven to other states.

485

486 *Running Published Methods*

487 To run t-SNE (14) a dimensionality reduction visualization tool, we utilized the scripts published here
488 (<https://lvdmaaten.github.io/tsne/>). Default settings were used.

489 To run SPADE, we first converted the simulated data to fcs format using Broad Institute's free
490 CSVtoFCS online tool in GenePattern(15) (<http://www.broadinstitute.org/cancer/software/genepattern#>).

491 Next, we carried out the tests using the SPADE package in Bioconductor R(16)
492 (<https://bioconductor.org/packages/release/bioc/html/spade.html>).

493 To run flowMeans, we carried out the tests using the flowMeans package in Bioconductor R(1)
494 (<https://bioconductor.org/packages/release/bioc/html/flowMeans.html>).

495 In the comparisons, we selected only cases that work for all methods to make the tests as fair as possible.

496 To calculate the mutual information of the subpopulations, we use the infotheo R package (<https://cran.r-project.org/web/packages/infotheo/index.html>).

498 To run network inference, we use the mnet algorithm in the parmigene R package (13). (<https://cran.r-project.org/web/packages/parmigene/index.html>).

500

501 *Code Availability*

502 The PAC R package can be accessed at:

503 <https://cran.r-project.org/web/packages/PAC/index.html>

504

505 *Simulated Data for Clustering Analysis*

506 To compare the clustering methods, we generated simulated data from Gaussian Mixture Model varying
507 dimension, the number of mixture components, mean, and covariance. The dimensions range from 5 to
508 39. The number of mixture components is varied along each dimension. The mean of each component

509 was generated uniformly from a d-dimensional hypercube; we generated datasets using hypercube of
510 different sizes, but kept all the other attributes the same. The covariance matrices were generated as AA^T ,
511 where A is a random matrix whose elements were independently drawn from the standard normal
512 distribution. The sizes of the simulated dataset range from 100k to 200k.

513 The simulated data are provided as (Datasets 1-6). Datasets 1-4 are for the PAC part. Dataset 1 contains
514 data with 5 dimensions; Dataset 2 contains data with 10 dimensions; Datasets 3a and 3b contain data with
515 20 dimensions; and Datasets 4a and 4b contain data with 35 dimensions. The ground truth labels are
516 included as separate sheets in each dataset.

517 When applying flowMeans, SPADE, and the PAC to the data, we preset the desired number of
518 subpopulations to that in the data to allow for direct comparisons.

519

520 *Gated Flow Cytometry Data*

521 Two data files were downloaded from the FlowCAP challenges(2). One data file is from the
522 Hematopoietic stem cell transplant (HSCT) data set; it has 9,936 cell events with 6 markers, and human
523 gating found 5 subpopulations. Another data file is from the Normal Donors (ND) data set; it has 60,418
524 cell events with 12 markers, and human gating found 8 subpopulations. The files are the first ('001') of
525 each dataset. These data files were all 1) compensated, meaning that the spectral overlap is accounted for,
526 2) transformed into linear space, and 3) pre-gated to remove irrelevant events. We used the data files
527 without any further transformation and filtering. When applying flowMeans, SPADE, and the PAC to the
528 data, we preset the desired number of subpopulations to that in the data to allow for direct comparisons.

529

530 *Gated Mass Cytometry Data*

531 Human gated mass cytometry data was obtained by gating for the conventional immunology cell types
532 using the mouse bone marrow data recently published(11). The expert gating strategy is provided as
533 Supporting Figure 1. The gated sample subset contains 64,639 cell events with 39 markers and 24
534 subpopulations and it is provided as Dataset 7.

535 To test the performance of different analysis methods, the data was first transformed using the $\text{asinh}(x/5)$
536 function, which is the transformation used prior to hand-gating analysis; For SPADE analysis, we utilize
537 the $\text{asinh}(x/5)$ option in the SPADE commands. The post-clustering results from flowMeans, SPADE, b-
538 PAC, and d-PAC were then subsetted using the indexes of gated cell events. These subsetted results are
539 compared to the hand-gated results.

540

541 *Simulated Data for MAN Analysis*

542 To test the linking of subpopulations, we generated simulated data from multivariate Gaussian with preset
543 signal levels and randomly generated positive definite covariance matrices. There are two cases, batch
544 effect and dynamic. Each simulated sample file has five dimensions, with two of these varying in levels;

545 these are the dimensions that are visualized. Dataset 5 contains the data for general batch effects case and
546 Dataset 6 contains the data for dynamic effects case. The ground truth labels are included as separate
547 sheets in each dataset.

548

549 *General batch scenario.* Sample 1 represents data from an old instrument (instrument 1) while sample 2
550 represents data from a new instrument (instrument 2). There are two subpopulations per sample. These
551 two subpopulations are the same, but their mean marker levels shifted higher up in sample 2 due to higher
552 sensitivity of instrument 2 (Figure 2b). The subpopulations have different underlying relationships
553 between the markers. In this simulated experiment, five markers were measured. Out of the five markers,
554 two markers show significant shift, and we focus on these two dimensions by 2-dimensional scatterplots.
555 In Figure 2b, the left subpopulation in sample 1 is the same as the left subpopulation in sample 2; the
556 same with the right subpopulation. The same subpopulations were generated from multivariate Gaussian
557 distributions with changing means with fixed covariance structure.

558 *Dynamic scenario.* Dynamic scenario models the treatment-control and perturbation studies. In the
559 simulation, we have generated two subpopulations that nearly converge over the time course (Figure 3a).
560 The researcher could lose the dynamic information if they were to combine the samples for clustering
561 analysis. The related subpopulations were generated from multivariate Gaussian distributions with
562 changing means with fixed covariance structure.

563

564 *Raw CyTOF Data Processing*

565 The researcher preprocesses the data to 1) normalize the values to normalization bead signals, 2) de-
566 barcode the samples if multiple barcoded samples were stained and ran together, and 3) pre-gate to
567 remove irrelevant cells and debris to clean up the data(10,17). Gene expressions look like log-normal
568 distributions(18); given the lognormal nature of the values, the hyperbolic arcsine transform is applied to
569 the data matrix to bring the measured marker levels (estimation of expression values) close to normality,
570 while preserving all data points. Often, researchers use the $\text{asinh}(x/5)$ transformation, and we use the same
571 transformation for the CyTOF datasets analyzed in this study.

572

573 *Mouse Tissue Data*

574 In the Spitzer et al., 2015 dataset(11), three mouse strains were grown, and cells were collected from
575 different tissues: thymus, spleen, small intestine, mesenteric lymph node, lung, liver, inguinal lymph
576 node, colon, bone marrow, and blood. In each experiment, 39 expression markers were monitored. The
577 authors used the C57BL6 mouse strain as the reference(11); the data was downloaded from Cytobank,
578 and we performed our analysis on the reference strain.

579 First, all individual samples were filtered by taking the top 95% of cells based on DNA content and then
580 the top 95% of cells based on cisplatin: DNA content allows the extraction of good-quality cells and
581 cisplatin level (low) allows the extraction of live cells. Overall, the top 90% of cell events were extracted.

582 The filtered samples were then transformed by the hyperbolic arcsine ($x/5$) function, and merged as a
583 single file, which contains 13,236,927 cell events and 39 markers per event (Supporting Table 2).

584 Using PAC-MAN, we obtained 35 subpopulations in each sample then 80 clades for the entire dataset.
585 The 80 clades account for the traditional immune subpopulations and sample-specific subpopulations.
586 Small subpopulations not used in alignment are later merged into the closest clades; this is done by
587 performing hierarchical clustering with the marker signals to obtain 5 “expression” subclades per sample.
588 Subsequently, any clade with less than 100 cells is discarded. Subpopulation proportion heatmap was
589 plotted to visualize the subpopulation-specificities and relationships across the samples. Finally,
590 annotation was performed using the hub markers of each representative subpopulation in each sample.

591

592 **Acknowledgements**

593 We thank the members of Wong Lab, in particular Tung-yu Wu, Chen-yu Tseng and Kun Yang, for
594 critical feedback.

595 This research was supported by the Stanford SIGF-BioX fellowship and the T32 GM007276 grant to
596 Y.H.L. and the NIH R01GM109836, NSF-DMS1330132, and NSF-DMS1407557 grants to W.H.W.

597

598 **References**

599

- 600 1. Aghaeepour N, Nikolic R, Hoos HH, Brinkman RR. Rapid cell population identification in flow
601 cytometry data. *Cytometry A*. 2011 Jan 1;79A(1):6–13.
- 602 2. Aghaeepour N, Finak G, Consortium TF, Consortium TD, Hoos H, Mosmann TR, et al. Critical
603 assessment of automated flow cytometry data analysis techniques. *Nat Methods*. 2013
604 Mar;10(3):228–38.
- 605 3. Qiu P, Simonds EF, Bendall SC, Gibbs Jr KD, Bruggner RV, Linderman MD, et al. Extracting a
606 cellular hierarchy from high-dimensional cytometry data with SPADE. *Nat Biotechnol*. 2011
607 Oct;29(10):886–91.
- 608 4. Wong WH, Ma L. Optional Pólya tree and Bayesian inference. *Ann Stat*. 2010 Jun;38(3):1433–59.
- 609 5. Lu L, Jiang H, Wong WH. Multivariate Density Estimation by Bayesian Sequential Partitioning. *J*
610 *Am Stat Assoc*. 2013 Dec 1;108(504):1402–10.
- 611 6. Yang K, Wong WH. Discovering and Visualizing Hierarchy in the Data. ArXiv14034370 Stat
612 [Internet]. 2014 Mar 18 [cited 2015 Nov 27]; Available from: <http://arxiv.org/abs/1403.4370>
- 613 7. Yang K, Wong WH. Density Estimation via Adaptive Partition and Discrepancy Control.
614 ArXiv14041425 Stat [Internet]. 2014 Apr 4 [cited 2015 Nov 27]; Available from:
615 <http://arxiv.org/abs/1404.1425>

- 616 8. Jiang H, Mu JC, Yang K, Du C, Lu L, Wong WH. Computational Aspects of Optional Pólya Tree. *J*
617 *Comput Graph Stat.* 2015 Feb 13;0(ja):00–00.
- 618 9. Samusik N, Good Z, Spitzer MH, Davis KL, Nolan GP. Automated mapping of phenotype space
619 with single-cell data. *Nat Methods.* 2016 Jun;13(6):493–6.
- 620 10. Finck R, Simonds EF, Jager A, Krishnaswamy S, Sachs K, Fantl W, et al. Normalization of mass
621 cytometry data with bead standards. *Cytometry A.* 2013 May 1;83A(5):483–94.
- 622 11. Spitzer MH, Gherardini PF, Fragiadakis GK, Bhattacharya N, Yuan RT, Hotson AN, et al. An
623 interactive reference framework for modeling a dynamic immune system. *Science.* 2015 Jul
624 10;349(6244):1259425.
- 625 12. Samusik N, Good Z, Spitzer MH, Davis KL, Nolan GP. Automated mapping of phenotype space
626 with single-cell data. *Nat Methods.* 2016 Jun;13(6):493–6.
- 627 13. Sales G, Romualdi C. *parmigene*—a parallel R package for mutual information estimation and gene
628 network reconstruction. *Bioinformatics.* 2011 Jul 1;27(13):1876–7.
- 629 14. Maaten L van der, Hinton G. Visualizing Data using t-SNE. *J Mach Learn Res.* 2008;9(Nov):2579–
630 605.
- 631 15. Reich M, Liefeld T, Gould J, Lerner J, Tamayo P, Mesirov JP. *GenePattern 2.0.* *Nat Genet.* 2006
632 May;38(5):500–1.
- 633 16. Linderman MD, Bjornson Z, Simonds EF, Qiu P, Bruggner RV, Sheode K, et al. *CytoSPADE:*
634 *high-performance analysis and visualization of high-dimensional cytometry data.* *Bioinformatics.*
635 2012 Sep 15;28(18):2400–1.
- 636 17. Zunder ER, Finck R, Behbehani GK, Amir ED, Krishnaswamy S, Gonzalez VD, et al. Palladium-
637 based mass tag cell barcoding with a doublet-filtering scheme and single-cell deconvolution
638 algorithm. *Nat Protoc.* 2015 Feb;10(2):316–33.
- 639 18. Bengtsson M, Ståhlberg A, Rorsman P, Kubista M. Gene expression profiling in single cells from
640 the pancreatic islets of Langerhans reveals lognormal distribution of mRNA levels. *Genome Res.*
641 2005 Oct 1;15(10):1388–92.
- 642
- 643

644 **Figure and Table Legends**

645

646 **Figure 1: PAC utilizes rational initialization for fast and accurate clustering convergence**

647 (a) Partition-based methods estimate data density by cutting the data space into smaller rectangles.
648 Bayesian Sequential Partition (BSP) divides the data space via binary partition in the middle of the
649 bounded region, while that of Discrepancy Sequential Partition (DSP) occur at the location that balances
650 the data point uniformly on both sides of the cut. The numbers denote sequential order of partitions. Since
651 DSP adapts to the data points, it converges on the estimated density faster than BSP. (b) In the (one-step)
652 look-ahead of version of partition, the algorithm cuts the data space for all potential cuts plus one step
653 more (steps 2 and 3), and it finds the optimal future version (after step 3), which determines the actual cut
654 (step 2). (c) The partitioning of simulated data space containing five subpopulations; the hyper-rectangles
655 surround high-density areas, approximating the underlying distribution. (d-e) The rational initialization
656 step helps PAC to outperform random initialization. The handgated CyTOF data was used. In this case,
657 the overall sum of squares error is lower and the F-measure is higher for PAC. (f) The convergence of
658 PAC toward the hand-gated results, or ground truth, is fast. It takes less than 50 downstream post-
659 processing kmeans iterations for the PAC to achieve a significantly higher F-measure than the alternative
660 methods. In contrast, flowMeans convergence is poor. (g) Visualization of clustering results with t-sne
661 plot. The t-sne plots contain 10,000 cell events of the handgated CyTOF data with different set of labels
662 drawn. Note that the colors are informative only within each panel. These labels are from kmeans,
663 SPADE, flowMeans, b-PAC, and d-PAC. The subpopulation numbers for all methods were set to be the
664 same as that of handgated results.

665

666 **Figure 2: Overlapping batch effects can be resolved by PAC-MAN**

667 (a) Schematic of MAN. Consider a deck of networks (in analogy to cards), with each “suit” representing a
668 sample and each “rank” representing a unique network structure. The networks are aligned by similarity
669 and organized on a dendrogram. The tree is cut (red line) at the user-specified level to output the desired k
670 clades. Within each clade, the network structures are similar or the same. If the same sample has multiple
671 networks in the same clade, then these networks are merged (black box around same cards). (b) Simulated
672 data samples with two of the same subpopulations. The means shifted due to measurement batch effect.
673 (c) When the samples are combined, as in the case of analyzing all samples together, two different
674 subpopulations overlap. (d) The overlapped subpopulations cannot be distinguished by clustering. (e)
675 PAC could be used to discover more subpopulations, however, the hints of the present of another
676 subpopulation do not help to resolve the batch effect. (f) PAC was used to discover several
677 subpopulations per sample without advanced knowledge of the exact number of subpopulations. (g) The
678 networks of the subpopulations discovered in (f). Networks can be grouped by similarities to organize the
679 subpopulations across samples; the alignment is based on Jaccard dissimilarity network structure
680 characterization matrix; dendrogram of the hierarchical clustering results. (h) Resolution of batch effect
681 by networks of all subpopulations discovered. (i) Resolution of batch effect first by gene networks of
682 larger subpopulations and then by merging smaller subpopulations into the aligned clades.

683

684 **Figure 3: Dynamic information can be extracted by PAC-MAN**

685 (a) Ground truth of simulated samples. Two subpopulations, in blue color, almost converge in time by
686 mean shifts. (b) PAC discovers several subpopulations per sample without advanced knowledge of the
687 number of subpopulations present. (c) Comparison of PAC-MAN results between representative clades
688 (number of clades set to 2). Using gene networks and expression information alone do not resolve the
689 dynamic information. On the other hand, dynamic information is resolved first by gene networks of larger
690 subpopulations and then by merging smaller subpopulations into the aligned clades.

691

692 **Figure 4: Mouse tissue data analysis results visualized by t-sne plots.**

693 Each t-sne plot was generated using 10,000 randomly drawn cell events from each mouse tissue sample.
694 The results from PAC (top panel) and MAN (bottom panel) steps are presented as a pair. Initial PAC
695 discovery was set to 35 subpopulations without advanced knowledge of the number of subpopulations in
696 each sample. In MAN, 80 network clades were outputted, and the cellular states are defined by gene
697 expression, network structure, and dataset-level variation. This composite definition naturally aggregates
698 the initial 35 subpopulations to yield smaller number of subpopulations in less variable samples.

699

700 **Figure 5: Clade proportions and annotation**

701 Heatmap of clade proportions across the samples. Sample-specific clades have a value of 1, while shared
702 clades have proportions spread across different samples. Physiologically similar samples share more
703 clades.

704

705 **Supporting Figure 1: Gating strategy of CyTOF data for methods comparison**

706 Biaxial gating hierarchy for the mouse bone marrow CyTOF dataset. Gating strategy that was used to find
707 24 reference populations in the mouse bone marrow CyTOF data. Pre-gating step involved removal of
708 doublets, dead cells, erythrocytes and neutrophils. Non-neutrophils population was either subject to
709 cluster analysis by computational tools or subsequent gating. Dotted boxes represent 24 terminal gates
710 that were selected as reference populations for the comparison analysis.

711

712 **Supporting Figure 2: Subpopulation purity of simulated and real CyTOF data**

713 (a) Subpopulation-specific purity plot of 35-dimensional simulated data with 10 subpopulations. The blue
714 points denote the differences between the p-measures of the partition-based method (either d-PAC or b-
715 PAC) and flowMeans, while the red points denote the p-measure differences between the partition
716 methods and SPADE. The horizontal line at 0 means no difference between the methods. Most of the blue

717 and red points are above 0, indicating that the PAC generates purer subpopulations compared to the
718 ground truth. The two subplots are very similar, which means that d-PAC and b-PAC give very similar p-
719 measures. More precisely, the sum of differences between d-PAC and flowMeans and d-PAC and
720 SPADE are 0.85 and 1.09, respectively; and the overall difference between b-PAC and flowMeans and b-
721 PAC and SPADE are 0.84 and 1.08, respectively.

722 (b) Subpopulation-specific purity plot of the hand-gated CyTOF data. The same convention is used as in
723 (Supporting Figure 2a). Again, more blue and red points are above 0, indicating that the partition-based
724 methods generate purer subpopulations compared to the ground truth. There is a cluster of points below 0
725 occurring in the middle of the plot, suggesting that flowMeans and SPADE capture the mid-size
726 subpopulations more similar to hand-gating than the partition-based methods. More specifically,
727 flowMeans does better (p-measure difference of 0.1 or better; difference of less 0.1 is considered
728 practically no difference) with finding subpopulations of GMP, CD8 T cells, MEP, CD4 T cells
729 (compared to d-PAC), and Plasma cells, while SPADE does better with CD19+IgM- B cells, NK cells
730 (compared to d-PAC), CD8 T cells, NKT cells, Basophils, Short-Term HSC, and Plasma cells. However,
731 overall, PAC has a much better performance, as the absolute sum of points above 0 is higher than that of
732 points below 0. More precisely, the sum of differences between d-PAC and flowMeans and d-PAC and
733 SPADE are 1.21 and 1.45, respectively; and the overall difference between b-PAC and flowMeans and b-
734 PAC and SPADE are 2.06 and 2.31, respectively. The difference table is provided in Supporting Table 1.

735

736 **Supporting Figure 3: Gene Networks inferred from subpopulations in the dynamic example** 737 **simulated dataset**

738 Figure 3 introduced the dynamic example in which five samples each having 2 true subpopulations
739 capture the almost-convergence of means. Here the underlying gene network structures for the PAC
740 discovered subpopulations (three per sample) are presented.

741

742 **Supporting Figure 4: Comparison between aligning cross-sample subpopulations by gene network,** 743 **expression profile, or both**

744 (a) PAC can be used to discover more subpopulations, with the effect of more partitions from the true
745 clusters. (b) When over-partitioning is present, gene network or gene expression profile alone cannot
746 resolve the dynamic (or batch) effects due to noisy covariance for small fragments of distributions.
747 However, first aligning the larger subpopulations with more stable covariance, and thus network
748 structures, and then merge in the smaller subpopulations by expression profile resolves the effects. (c) If
749 more irrelevant edges were introduced, network alignment would fail due to the negative impact of the
750 miscellaneous edges; however, eliminating small subpopulations from the alignment step alleviates the
751 increased edge count problem.

752

753 **Supporting Figure 5: PAC-MAN style linkage by means**

754 (a) t-sne plots of mouse tissue samples colored by representative subpopulations labels from linkage by
755 means. (b) Subpopulation proportion heatmap of clades of samples from linkage by means.

756

757 **Supporting Figure 6: Comparison between network and means PAC-MAN**

758 (a) PAC-discovered subpopulations are aggregated by MAN into clades; the number of PAC
759 subpopulations/clades for the network and means PAC-MAN approaches are plotted. (b) After
760 aggregating shared clades within samples, the number of shared clades for the entire dataset is plotted for
761 the two PAC-MAN approaches. c) Using the network approach results as basis, the clades with strong
762 agreement (high p-measures) with the means PAC-MAN approach are given. The shared clades (present
763 in more than one sample) are reliable candidates for future experiment to find cross-sample relationships.

764

765 **Table 1: F-measure Comparisons of Methods on Simulated and Hand-gated Cytometry Datasets.**

766 F-measure is calculated using the original hand-gate labels and the estimated labels generated by each
767 analysis method. The true-positives are found if the methods assign the same labels to points belonging to
768 the same subpopulation in the hand-gated data. The more true-positives found, the higher the F-measure,
769 which ranges from 0 to 1, with 1 being the highest. Partition-based methods perform consistently well on
770 data ranging from 5 to 39 dimensions. In the simulations, d-PAC and b-PAC perform just as well or better
771 than flowMeans and SPADE. flowMeans gives drastically different F-measures for the cases
772 20_10_40_100k and 20_20_40_100k : 0.25386 vs. 0.92518; this large difference is likely due to the
773 random initiation of cluster centers. In the hand-gated datasets, SPADE has the worst performance.
774 Ultimately, the performance of flowMeans and SPADE deteriorate for the 39-dimensional real CyTOF
775 data, while d-PAC and b-PAC perform consistently well.

776 *Simulated data have the following convention: a_b_c_d, where a denotes the number of
777 dimensions/markers, b denotes the number of subpopulations, c denotes the size of the hypercube for data
778 generation, and d denotes the number of cells.

779 **from rounding up, not originally 1.00

780

781 **Supporting Table 1: Purity (p) Measure Differences in CyTOF Comparison**

782 p-measure differences in gated CyTOF data analysis comparison. The differences are shown for all the
783 annotated cell subpopulations, which are ordered by their sizes. Overall, the PAC methods give more
784 positive p-measures.

785

786 **Supporting Table 2: Sample Sizes in Mouse Tissue CyTOF Dataset**

787 The numbers of cells in the samples of Spitzer et al., 2015 CyTOF dataset. The data is from the C57BL6
788 mouse strain and a total of ten tissue samples are present. The raw column shows the number of cells

789 prior to filtering by DNA and cisplatin values. The final cell counts are shown in the filtered file (3rd)
790 column.

791

792 **Supporting Table 3: PAC-MAN Subpopulation Characterization Output for Mouse Tissue CyTOF**
793 **Dataset**

794 The full set of annotated results, along with mean expressions, subpopulation proportion and counts, are
795 reported.

796

797 **Supporting Table 4: Network-justified and means-justified p-measures for Alignments of PAC-**
798 **discovered Subpopulations**

799 The PAC-discovered subpopulations were mapped as clades in both the network and means PAC-MAN
800 approaches. The p-measures were calculated for the cases 1) network approach mapping as the basis and
801 2) means approach mapping as the basis. The comparison is the same in principle to the comparison of
802 labels for clustering methods. The results are ordered by p-measures.

803

Figure 1

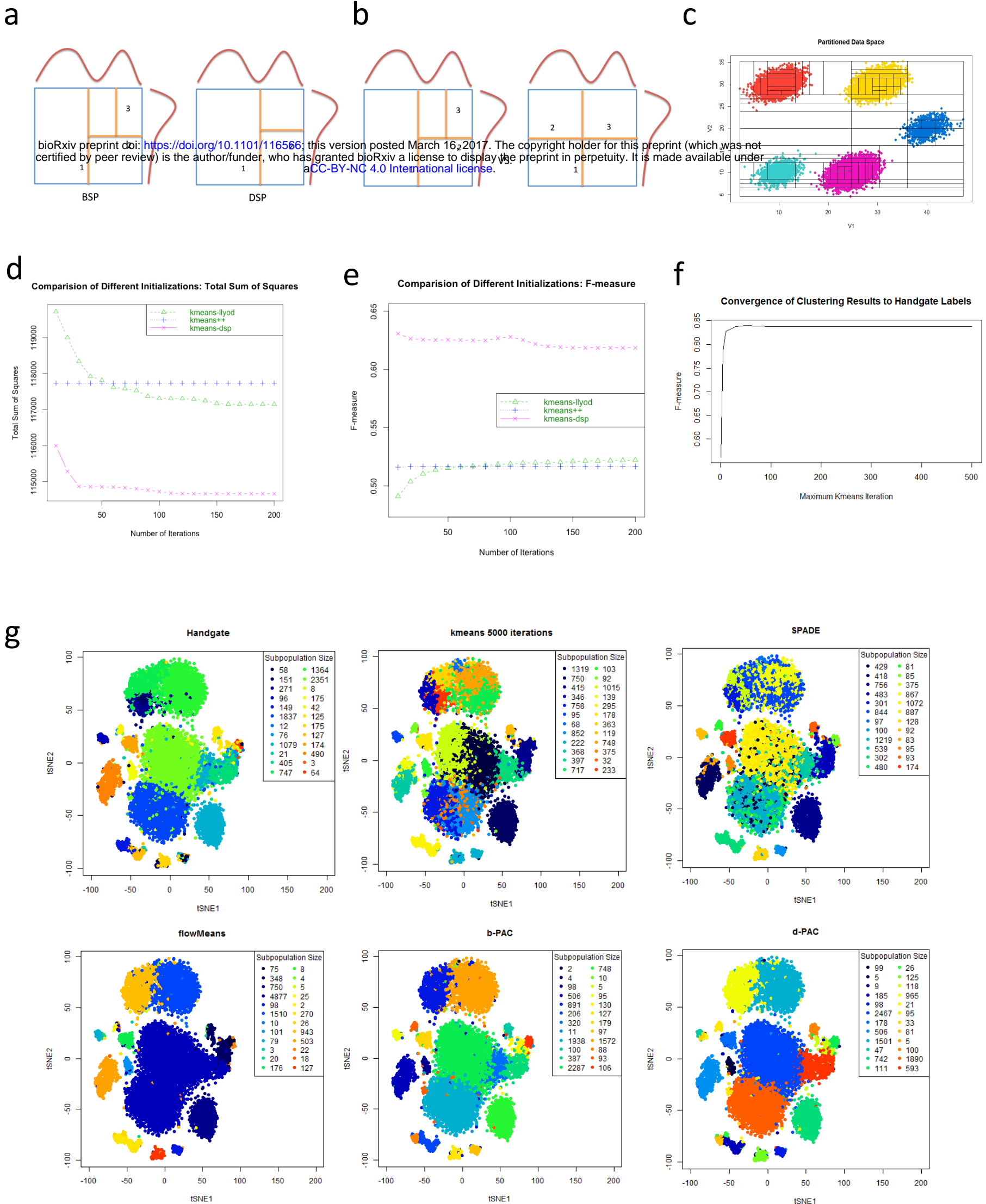


Figure 2

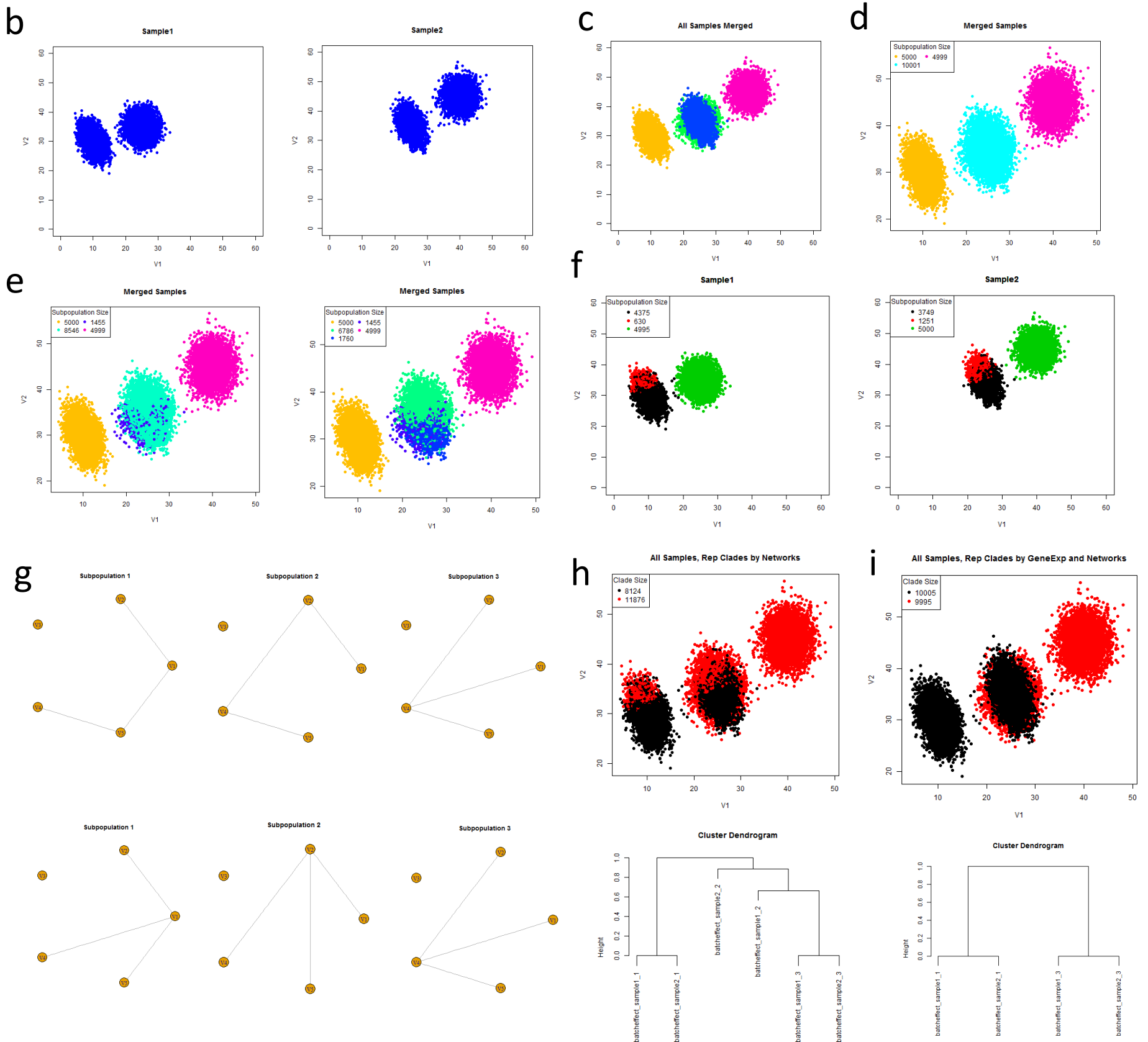
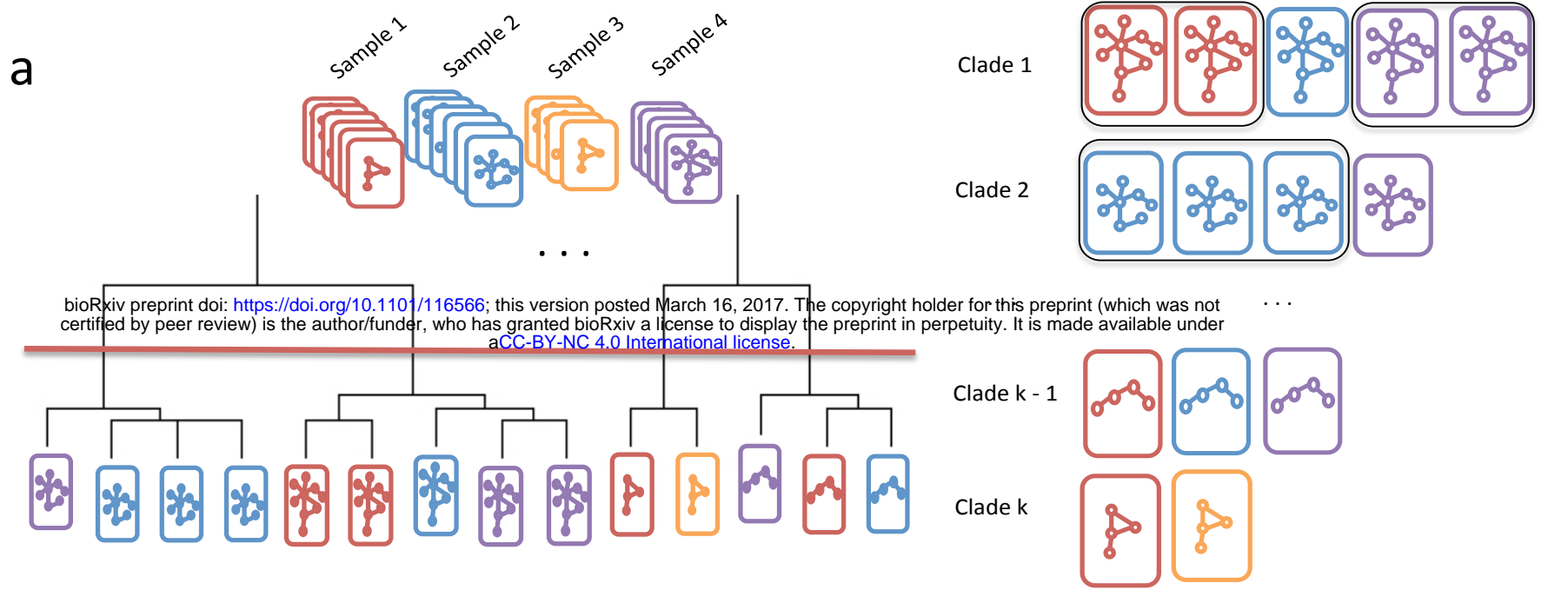
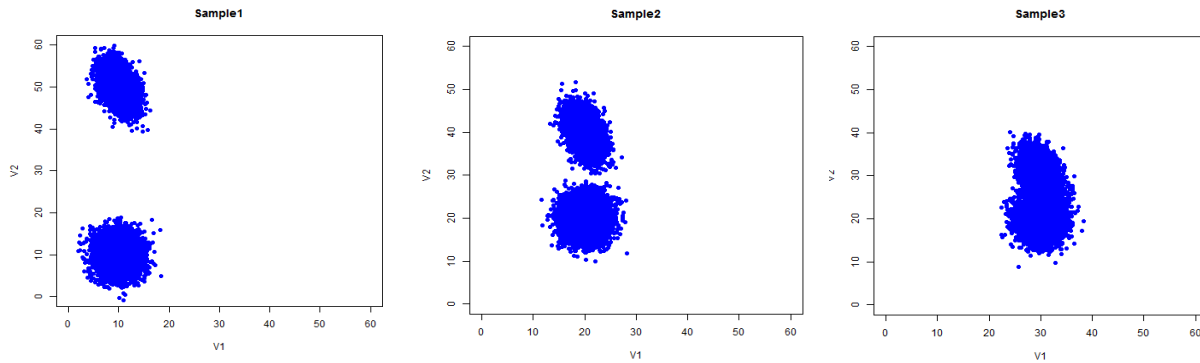
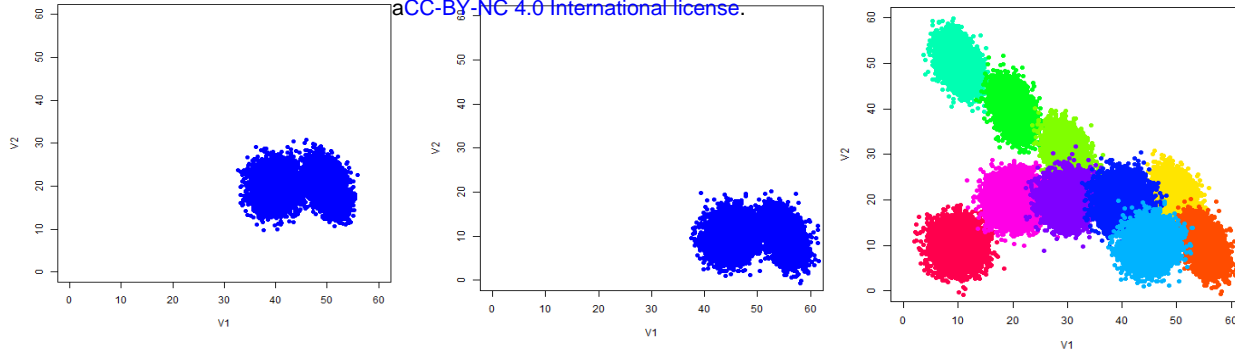


Figure 3

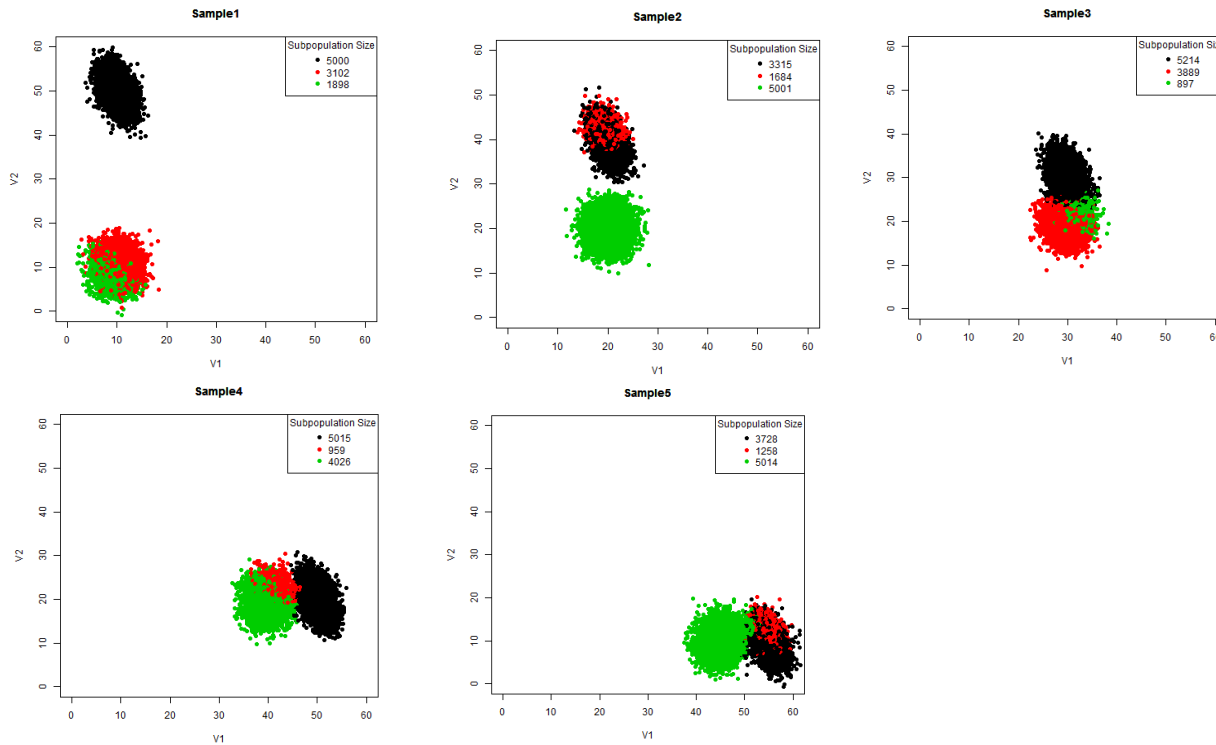
a



bioRxiv preprint doi: <https://doi.org/10.1101/116566>; this version posted March 16, 2017. The copyright holder for this preprint (which was not certified by peer review) is the author/funder, who has granted bioRxiv a license to display the preprint in perpetuity. It is made available under aCC-BY-NC 4.0 International license.



b



c

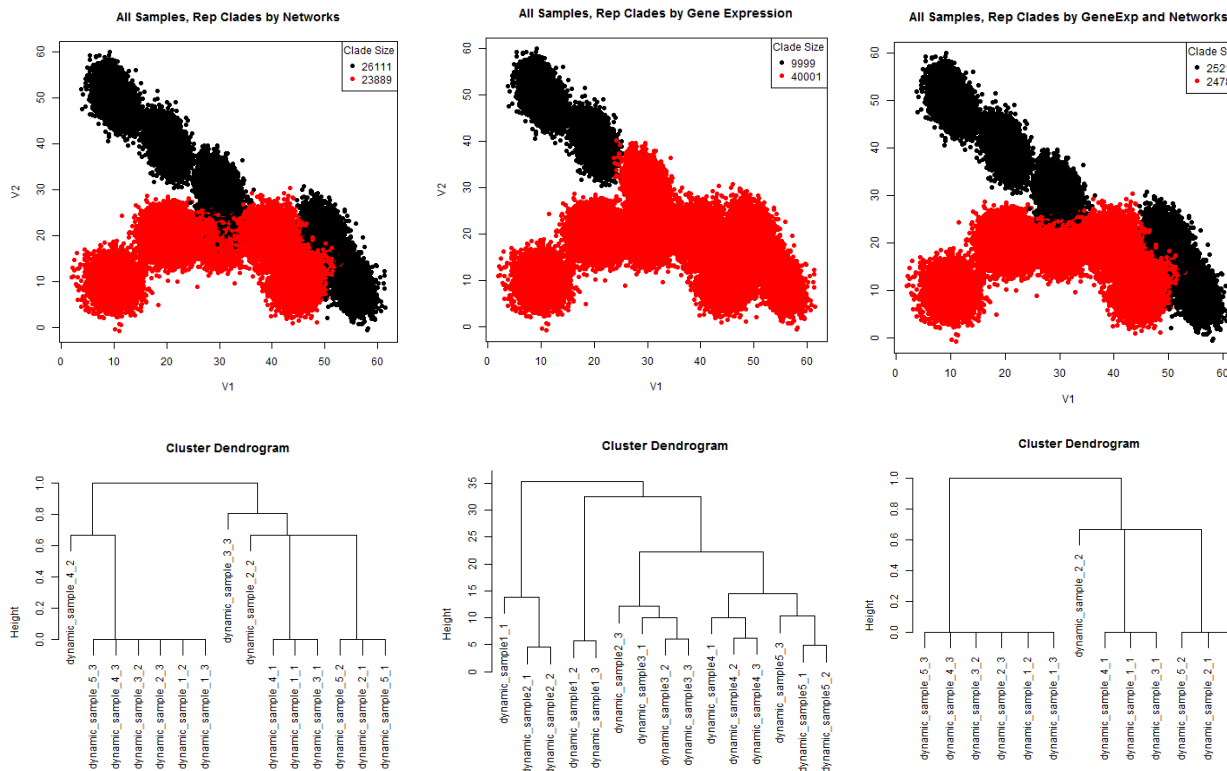


Figure 4

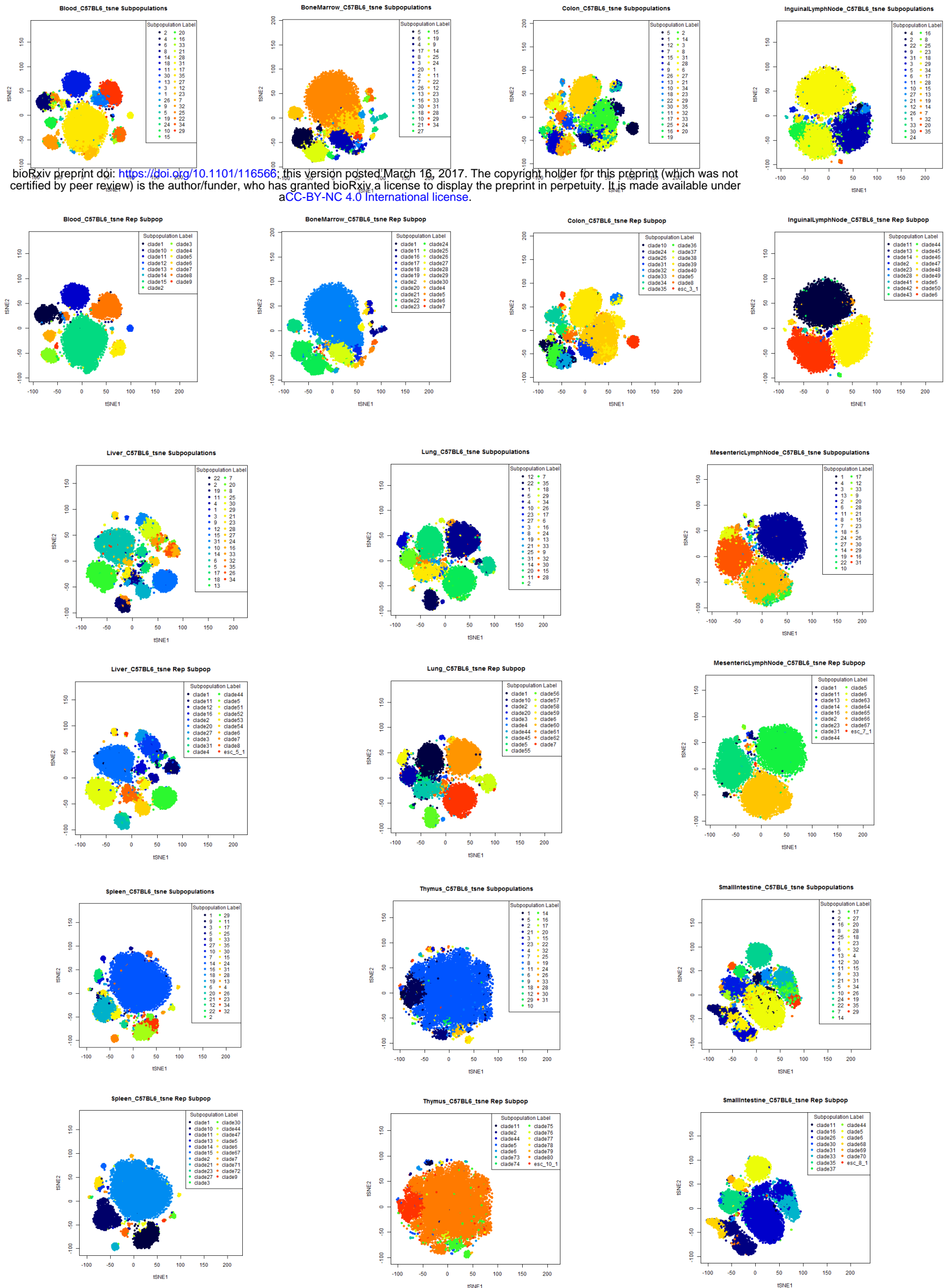
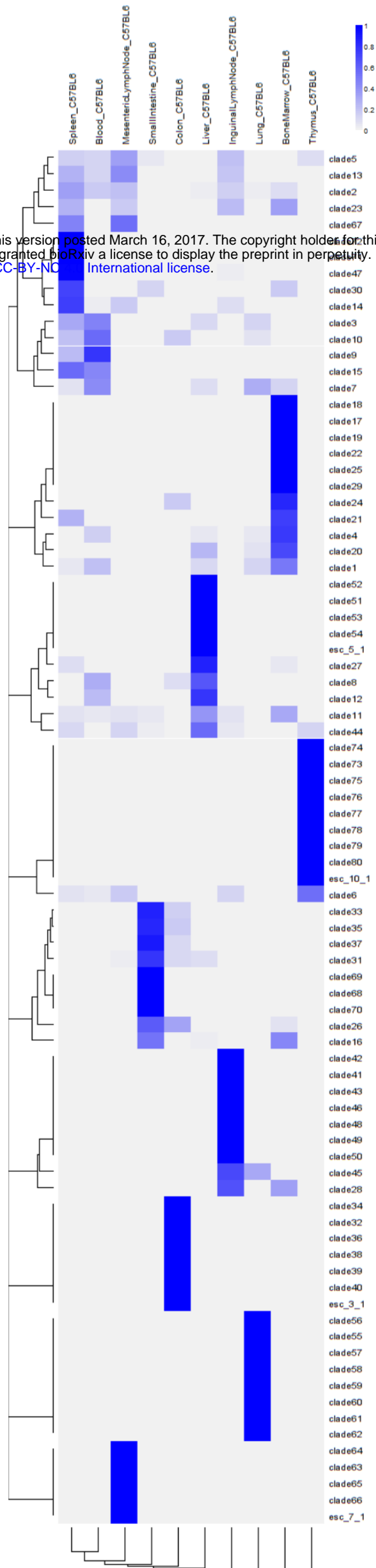


Figure 5

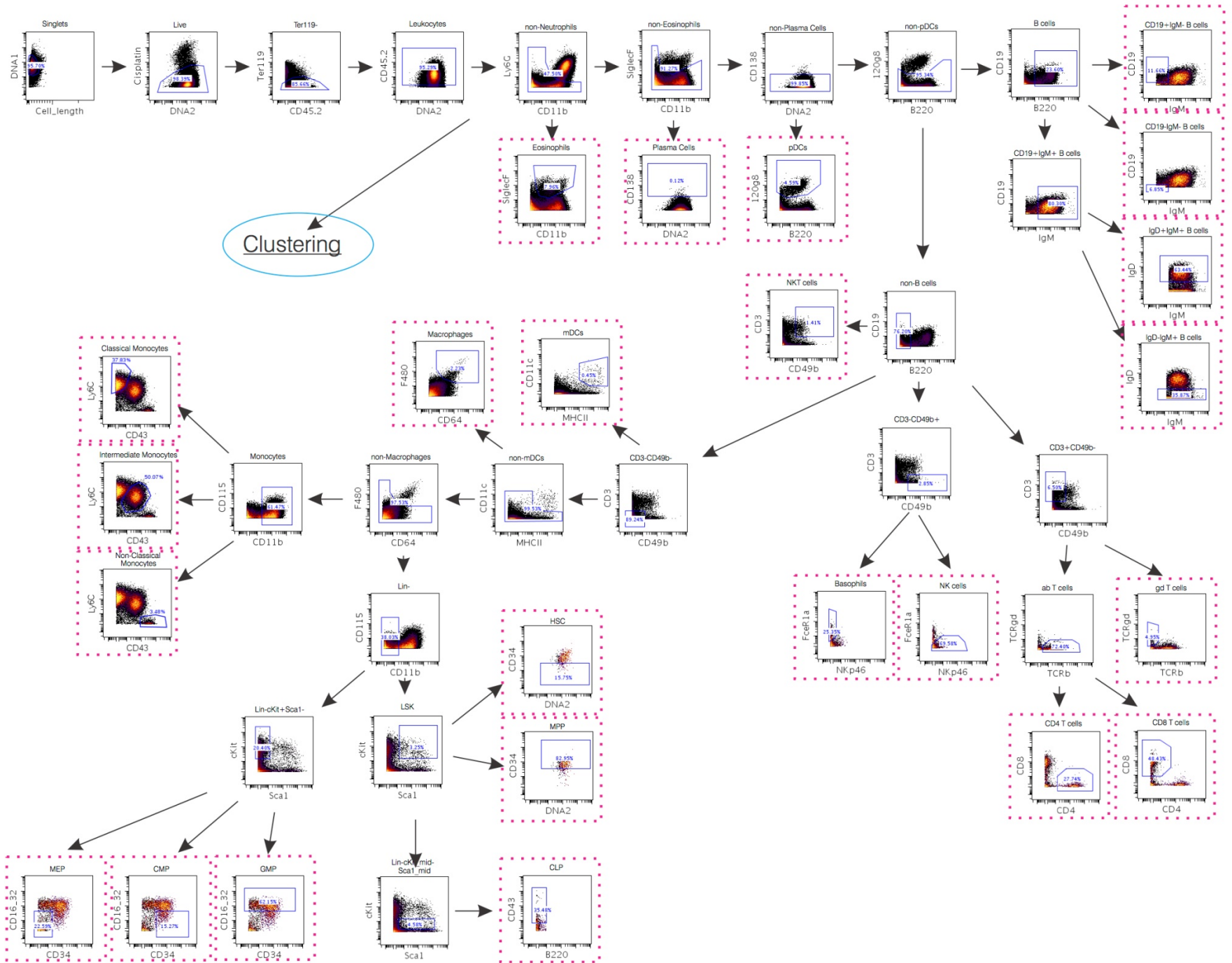


bioRxiv preprint doi: <https://doi.org/10.1101/116566>; this version posted March 16, 2017. The copyright holder for this preprint (which was not certified by peer review) is the author/funder, who has granted bioRxiv a license to display the preprint in perpetuity. It is made available under aCC-BY-NC-ND 4.0 International license.

Supporting Figure 1

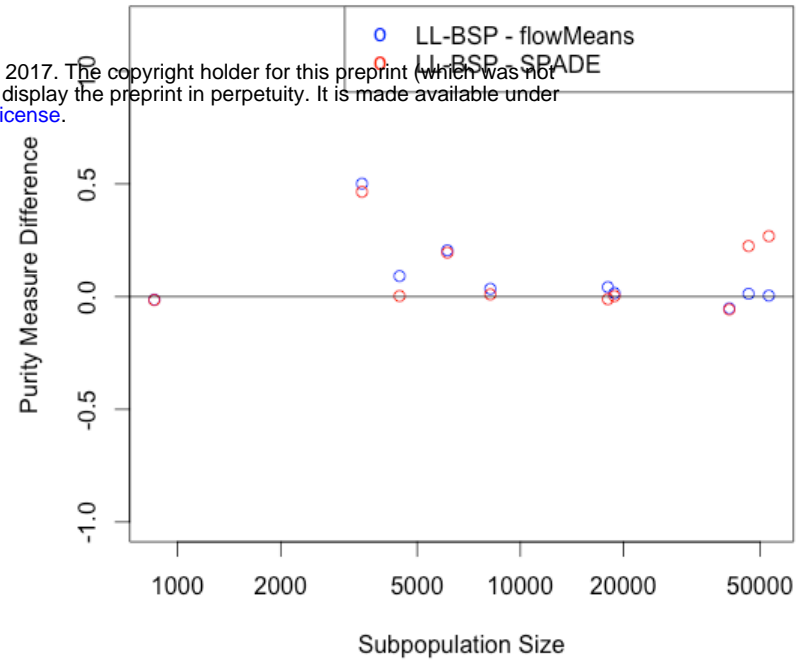
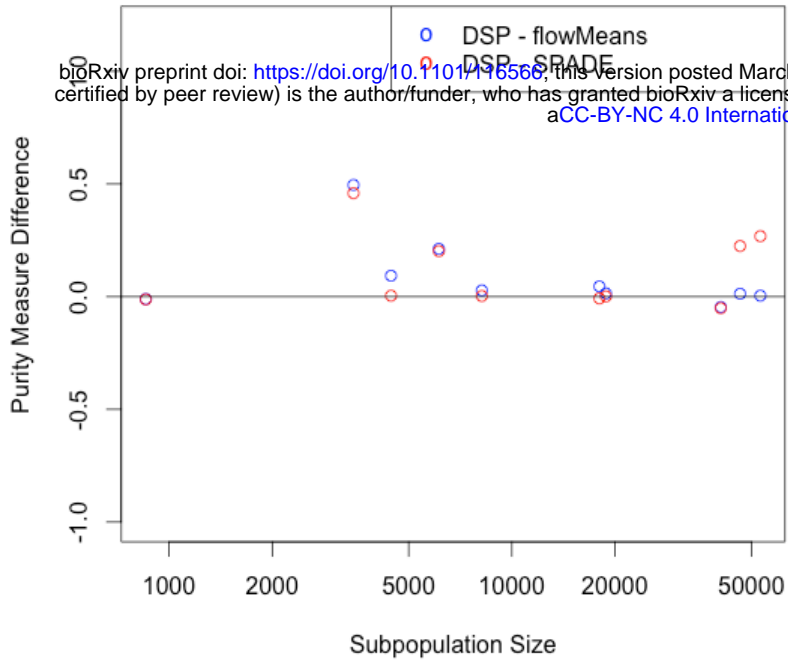
bioRxiv preprint doi: <https://doi.org/10.1101/116566>; this version posted March 16, 2017. The copyright holder for this preprint (which was not certified by peer review) is the author/funder, who has granted bioRxiv a license to display the preprint in perpetuity. It is made available under aCC-BY-NC 4.0 International license.

Pre-gating

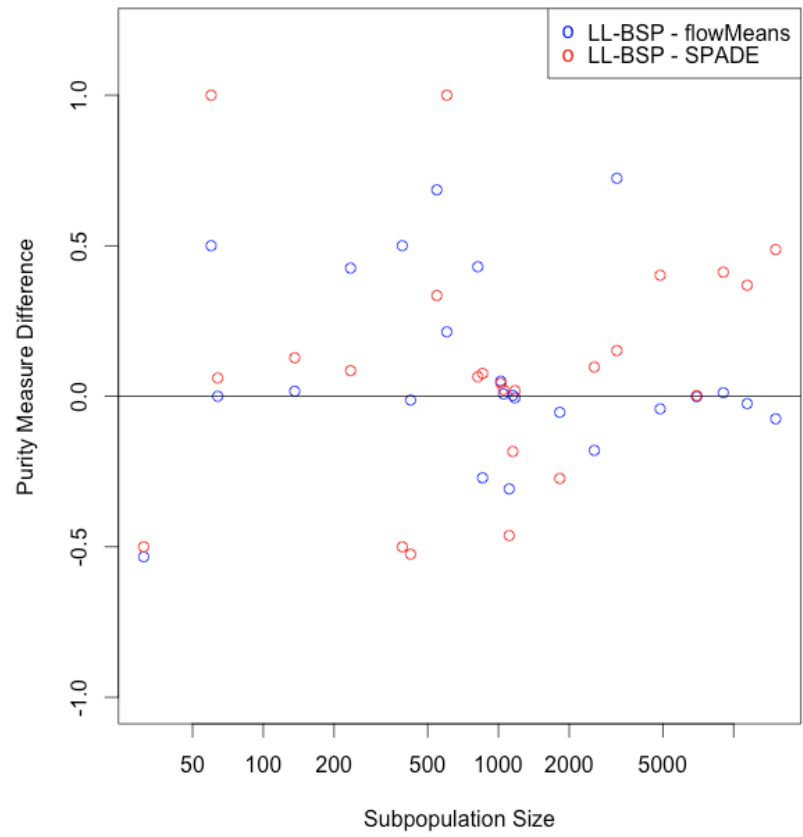
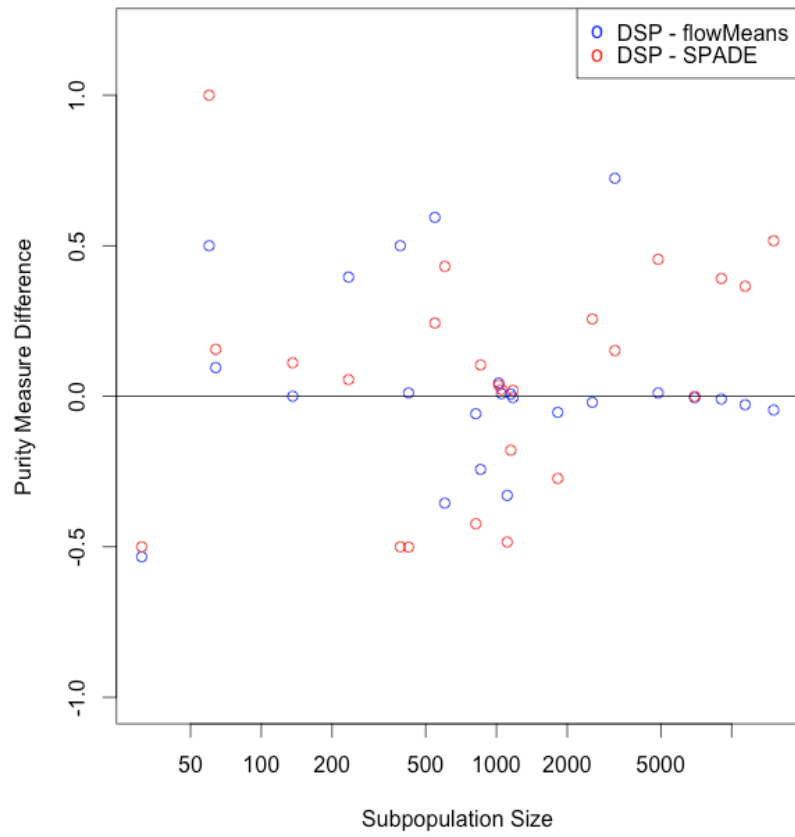


Supporting Figure 2

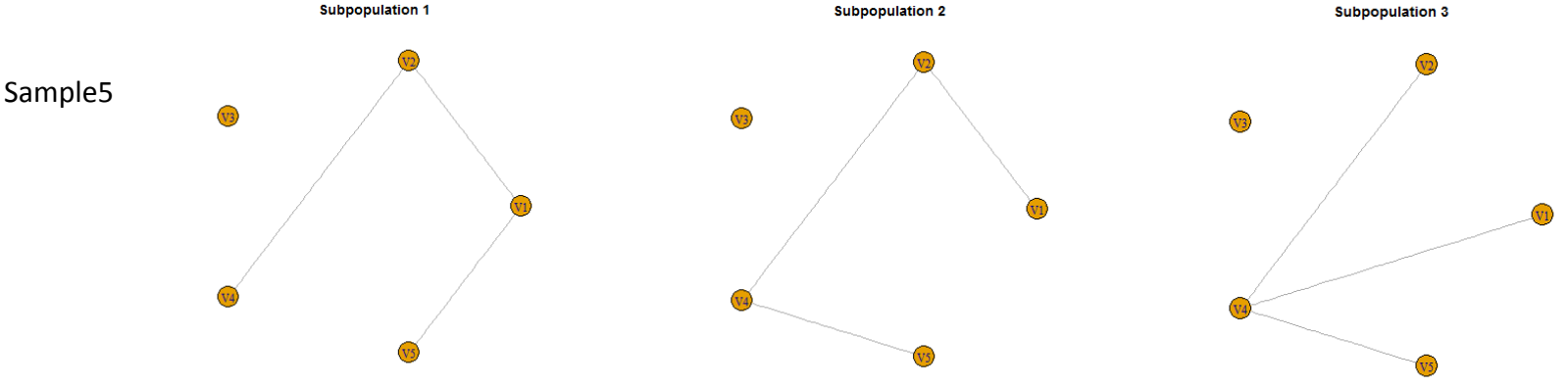
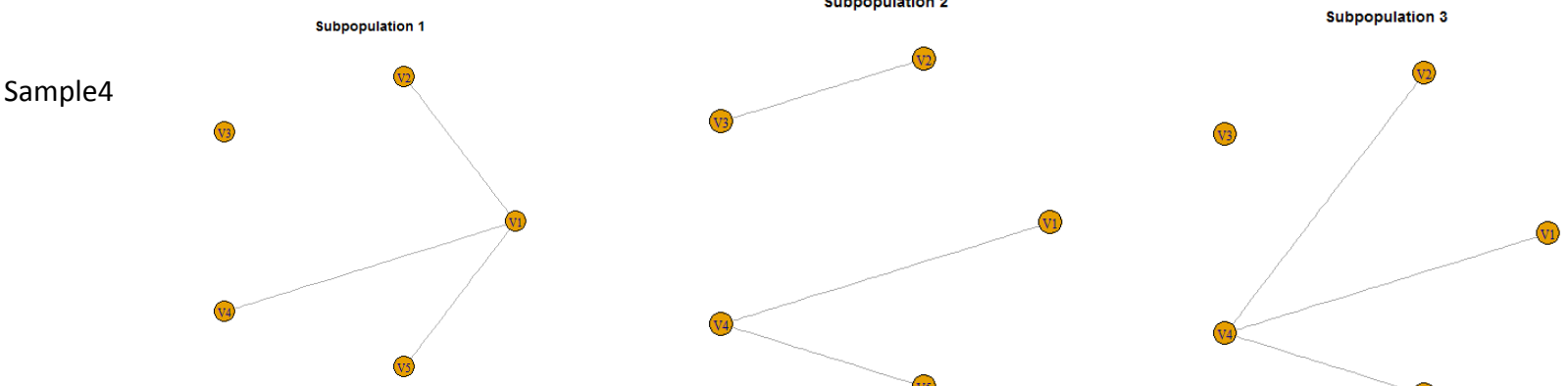
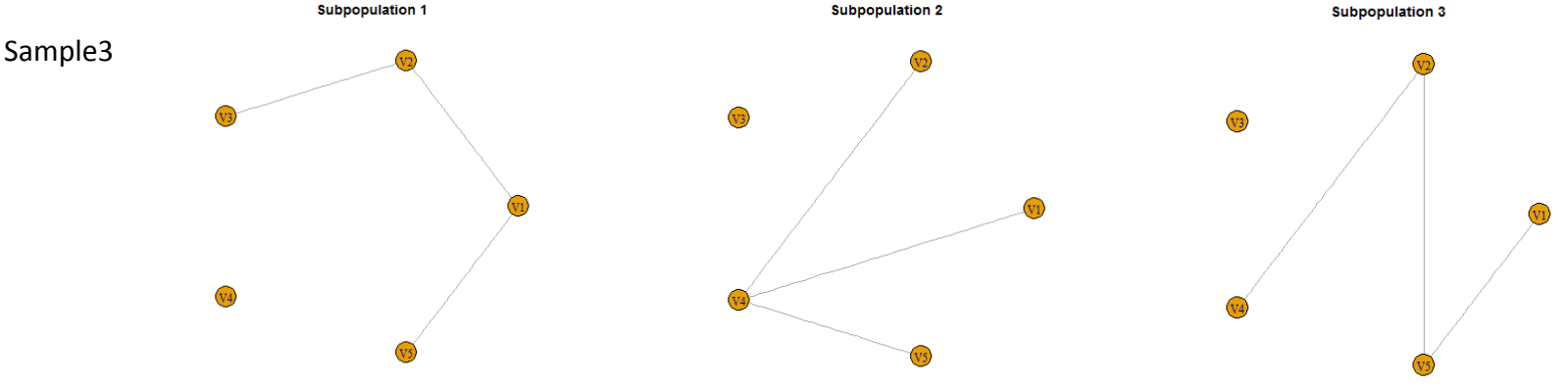
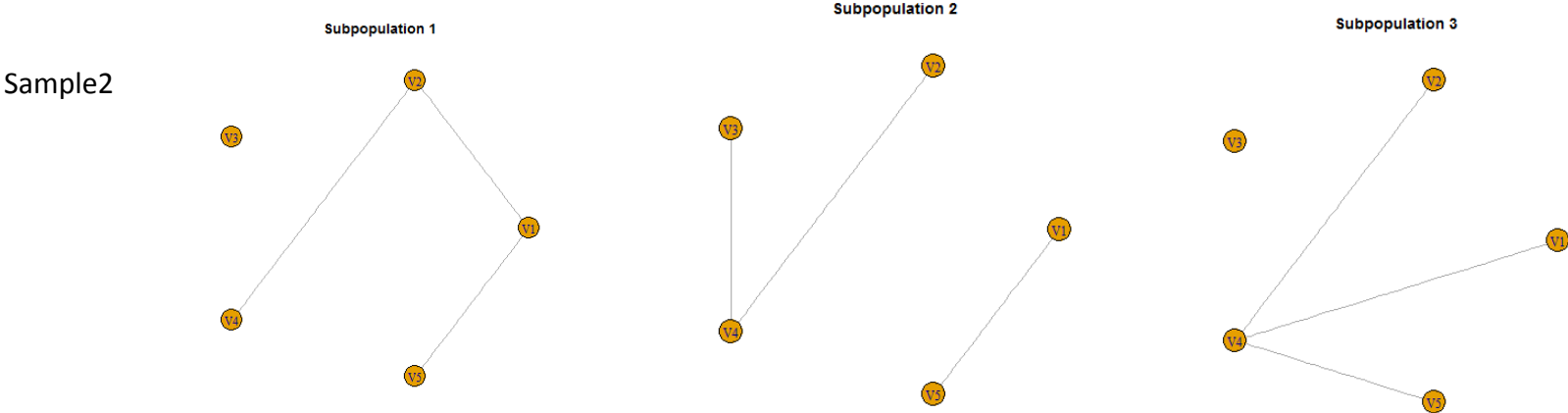
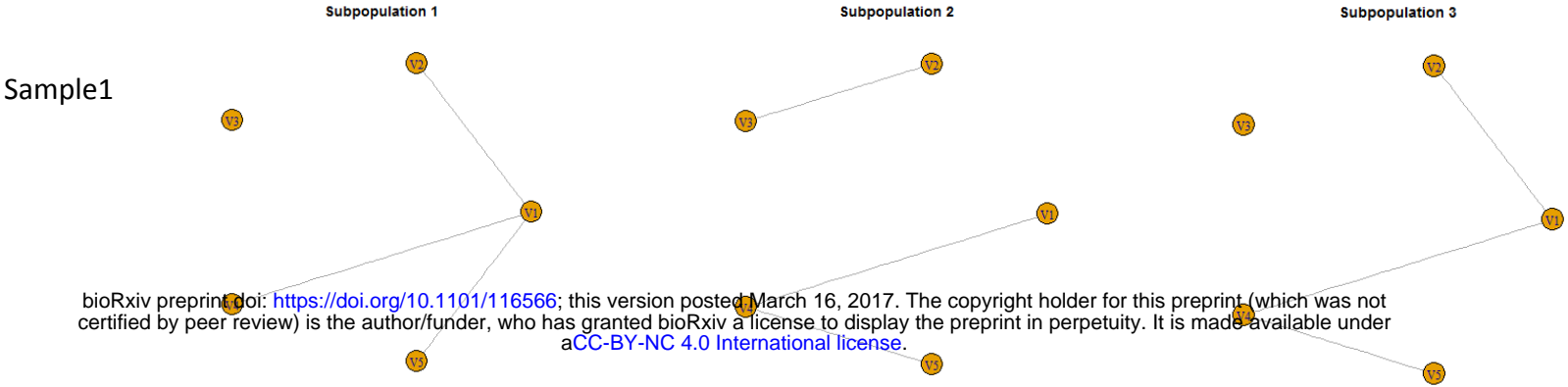
a



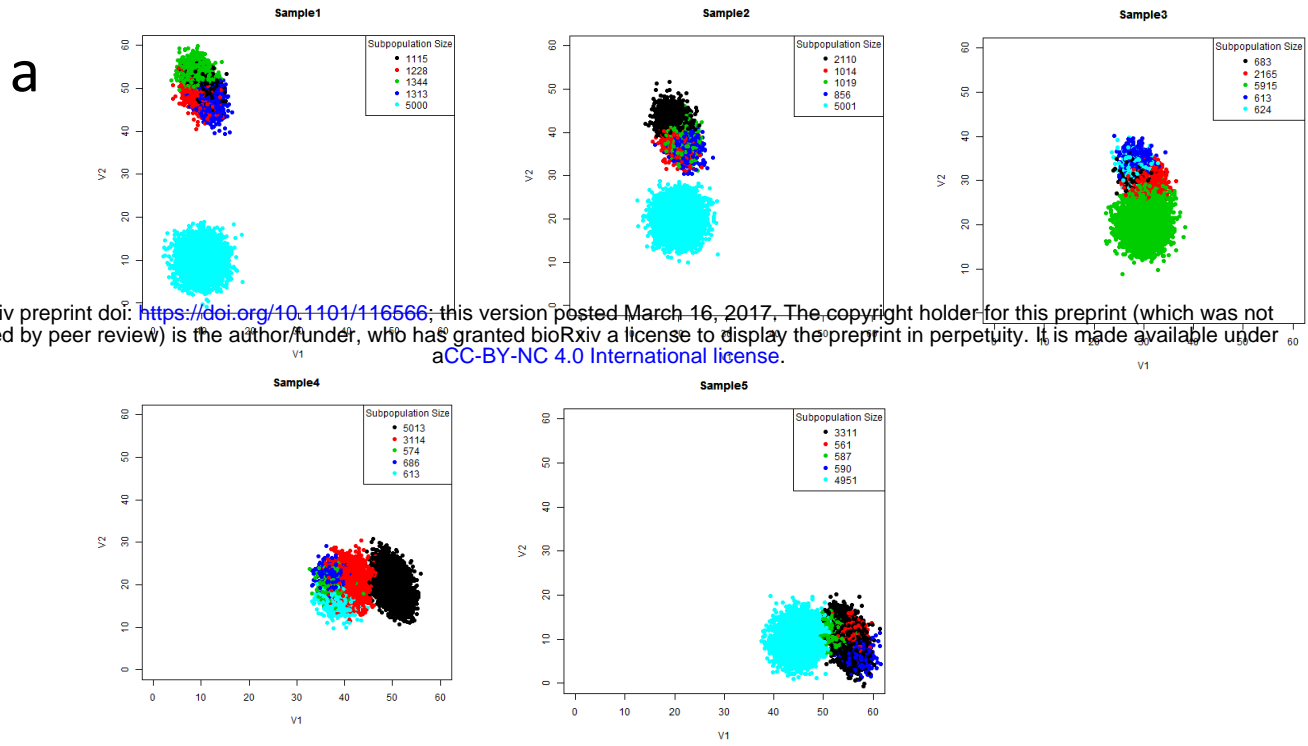
b



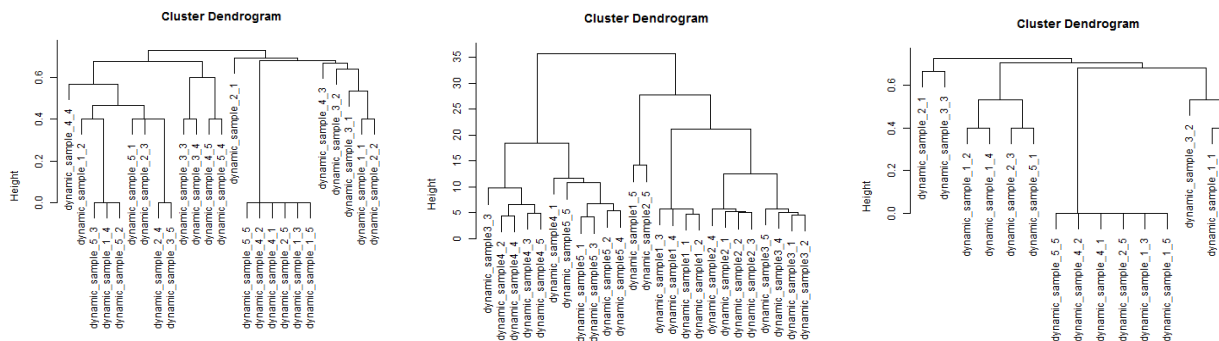
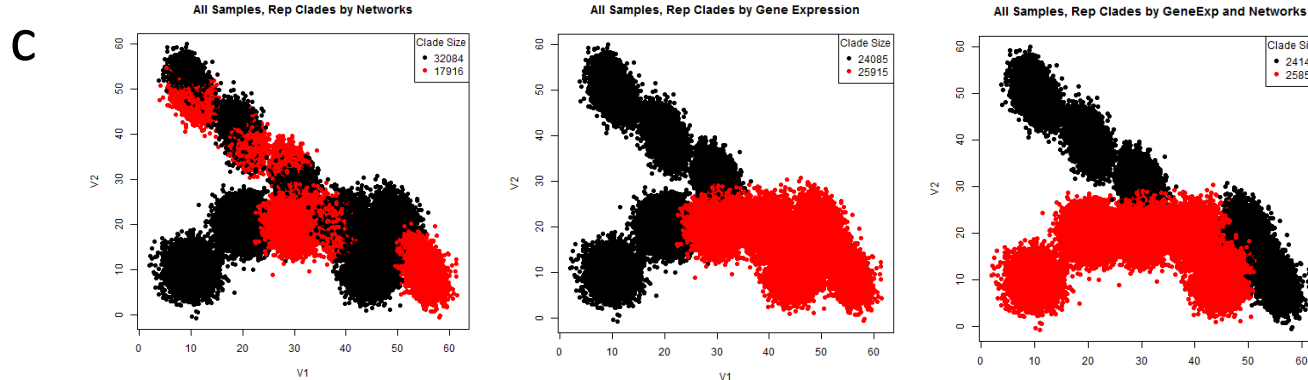
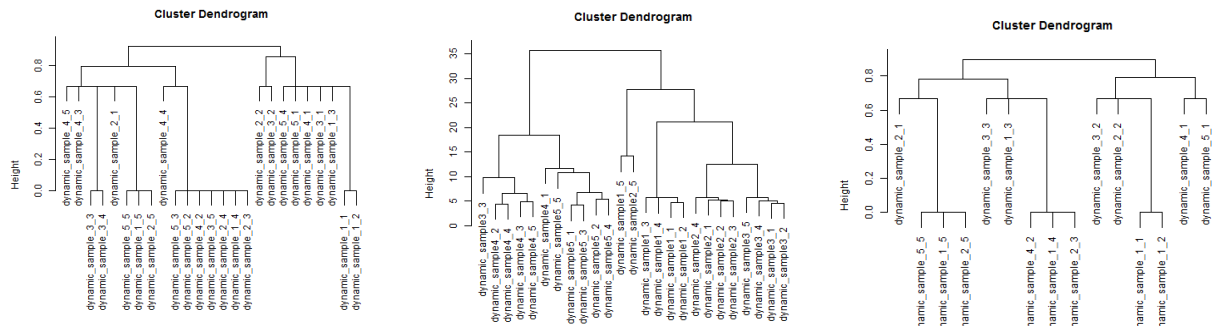
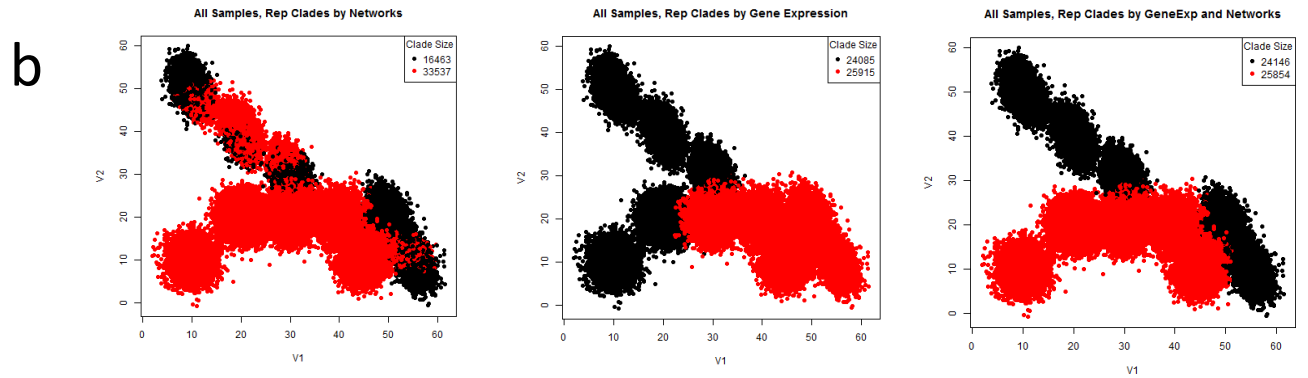
Supporting Figure 3



Supporting Figure 4

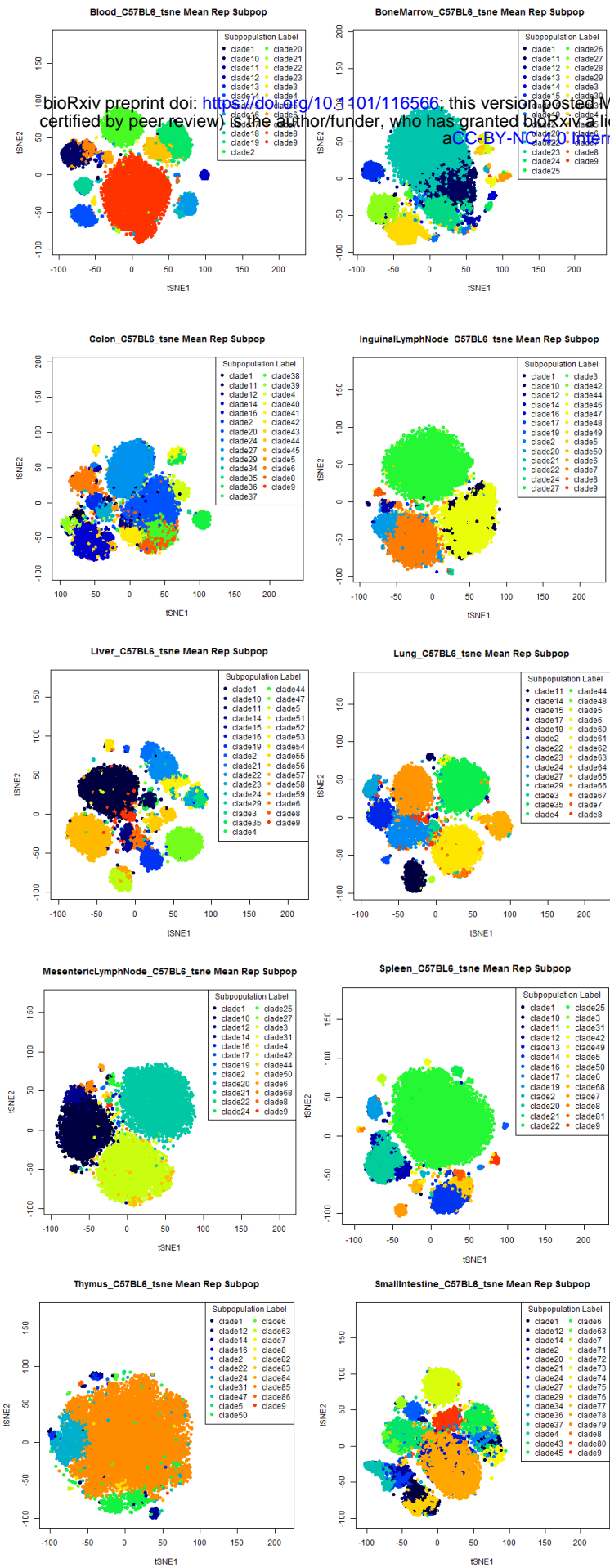


bioRxiv preprint doi: <https://doi.org/10.1101/116566>; this version posted March 16, 2017. The copyright holder for this preprint (which was not certified by peer review) is the author/funder, who has granted bioRxiv a license to display the preprint in perpetuity. It is made available under aCC-BY-NC 4.0 International license.

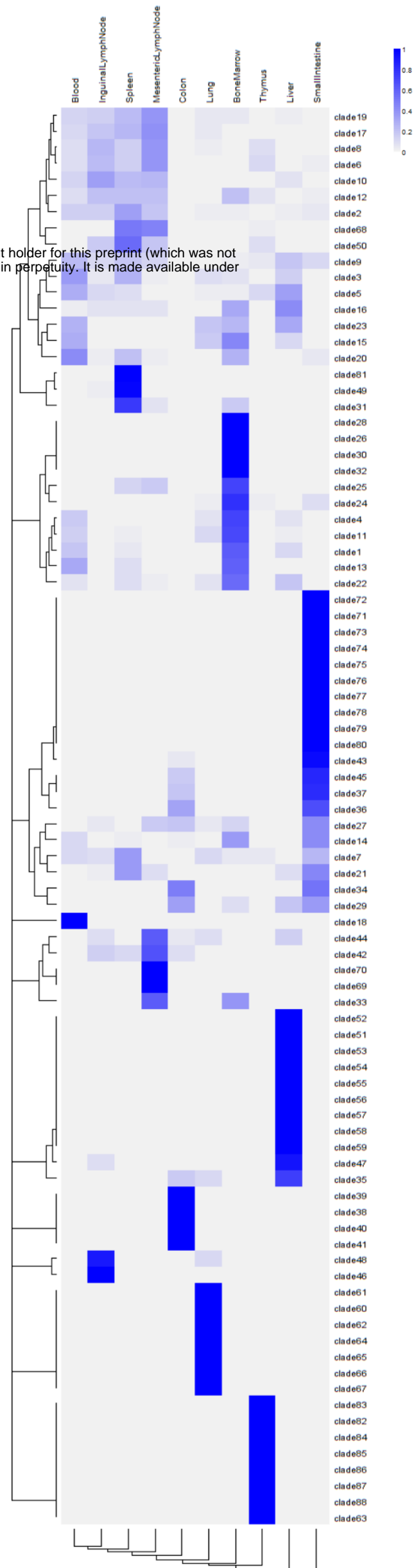


Supporting Figure 5

a

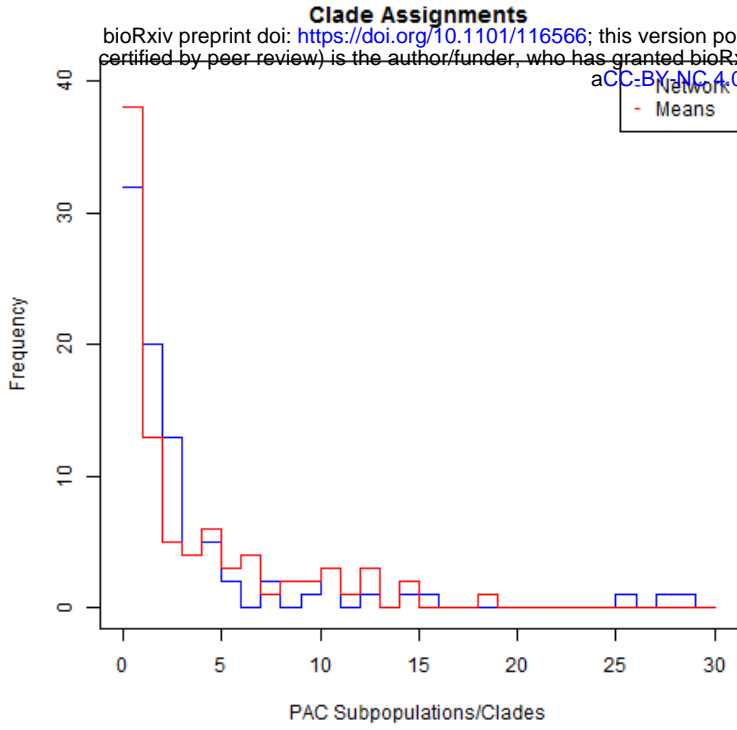


b

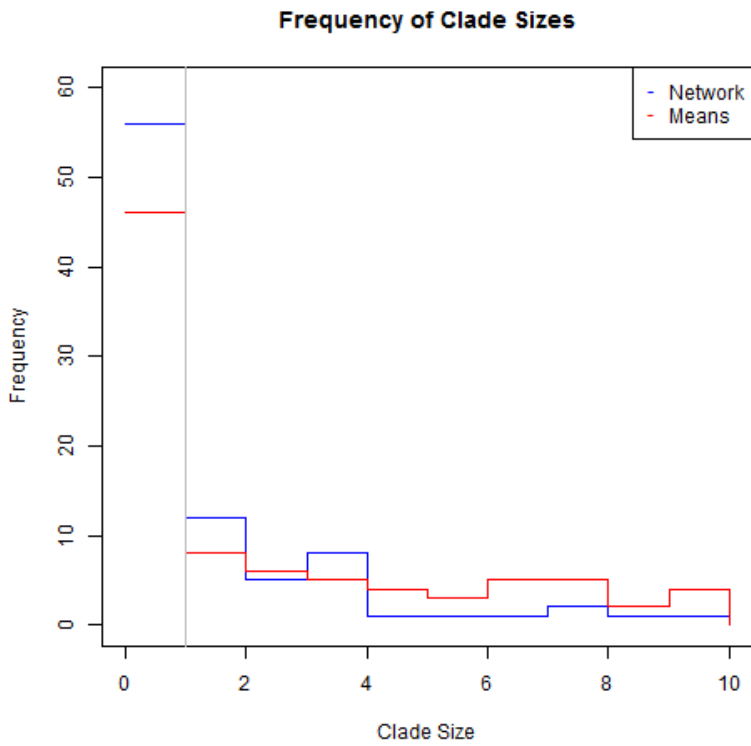


Supporting Figure 6

a



b



c

Clade	Number of PAC Subpop	n-measure	Dataset-level Proportion	Number of Samples Present
clade1	1	1	0.826687342	4
clade2	2	1	0.076407462	2
clade3	1	1	0.031185486	2
clade4	1	1	1.283666519	4
clade5	5	1	0.277964818	1
clade6	2	1	0.063776132	1
clade7	1	1	0.000339958	1
clade8	2	1	0.000377731	1
clade9	2	1	0.010417826	1
clade10	4	0.75	0.0216689266	2
clade11	15	0.73333	0.065861208	1
clade12	3	0.66667	0.027634813	1
clade13	8	0.5	0.001442933	1
clade14	11	0.36364	0.007660388	1
clade15	2	1	0.007660388	1
clade16	5	1	0.034947688	1
clade17	2	0.5	0.043590178	2
clade18	3	0.5	0.023426888	1
clade19	2	1	0.291140081	2
clade20	1	1	0.004026614	1
clade21	1	1	0.043907472	1
clade22	1	1	0.015026146	1
clade23	1	1	0.015026146	1
clade24	2	0.5	0.000695025	1
clade25	3	0.66667	0.614742379	1
clade26	1	1	0.090496835	1
clade27	1	1	0.008151439	1
clade28	3	0.66667	0.002266387	1
clade29	3	0.66667	0.013688978	1
clade30	4	0.75	0.084717548	3
clade31	15	0.73333	0.645202621	8
clade32	3	0.66667	0.117451732	3
clade33	3	0.66667	0.065249283	2
clade34	3	0.66667	0.052648171	1
clade35	3	0.66667	0.038407706	2
clade36	10	0.5	2.813553327	6
clade37	10	0.5	0.297402864	4
clade38	8	0.5	0.138785989	4
clade39	8	0.5	0.110365495	1
clade40	2	0.5	0.276642759	1
clade41	3	0.5	0.22283873	2
clade42	2	0.5	0.015328331	1
clade43	2	0.5	0.022920728	1
clade44	4	0.5	0.81990329	1
clade45	2	0.5	0.030180721	1
clade46	26	0.42308	24.41300764	9
clade47	29	0.41379	14.76349458	10
clade48	5	0.4	0.030074956	1
clade49	11	0.36364	10.7864008	4
clade50	11	0.36364	0.371619485	4
clade51	28	0.35714	29.79685542	8
clade52	6	0.33333	1.545260467	3
clade53	6	0.33333	0.567828167	2
clade54	3	0.33333	0.174889534	1